A STUDY OF BOILING WATER FLOW REGIMES AT LOW PRESSURE

Mario P. Fiori
Arthur E. Bergles

February, 1966

Report No. 5382-40
Contract AF 49(638)-1468

Department of
Mechanical Engineering
Massachusetts Institute
of Technology

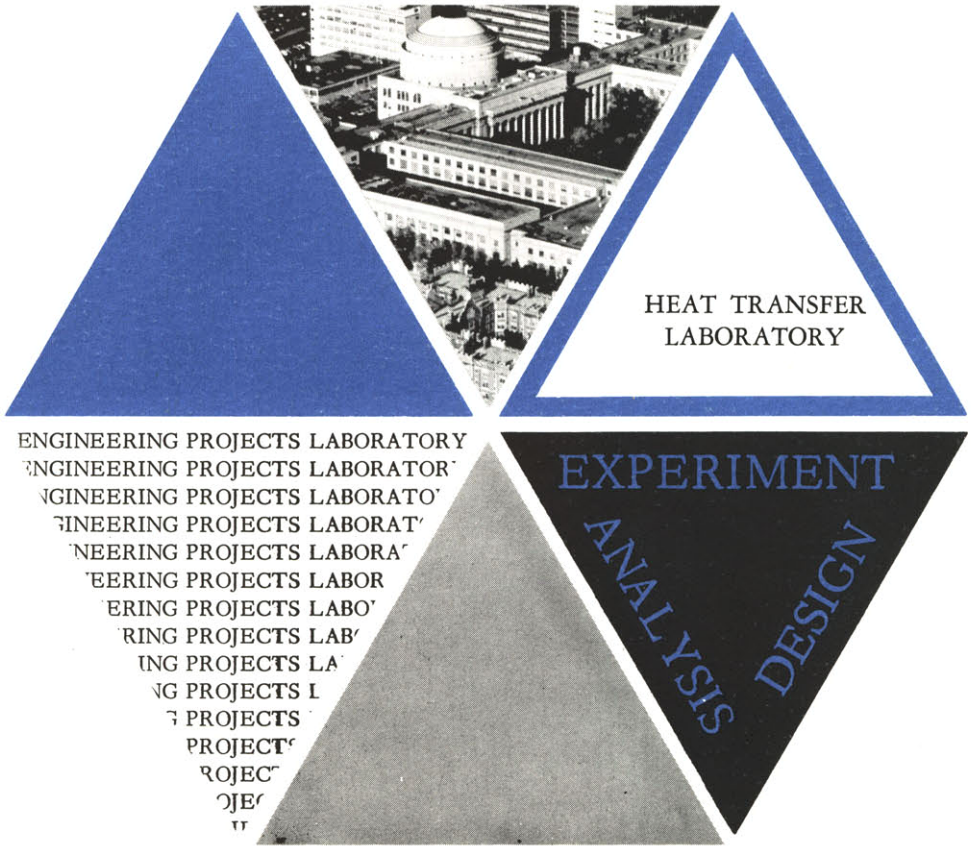

TECHNICAL REPORT NO. 5382-40

A STUDY OF BOILING WATER FLOW REGIMES AT LOW PRESSURE

by

Mario P. Fiori

Arthur E. Bergles

for

Massachusetts Institute of Technology

National Magnet Laboratory

Sponsored by the Solid State Sciences Division

Air Force Office of Scientific Research (OAR)

Air Force Contract AF 49(638)-1468

D.S.R. Project No. 5382

February, 1966

Department of Mechanical Engineering

Massachusetts Institute of Technology

Cambridge, Massachusetts 02139

ABSTRACT

A comprehensive experimental program to examine flow regimes at pressures below 100 psia for boiling of water in tubes was carried out.

An electrical probe, which measures the resistance of the fluid between the centerline of the flow and the tube wall, was used to identify the various flow regimes. This probe proved to be an ideal detection device, because of its simplicity, reproducibility, and accurate representation of the flow pattern within the heated test section.

The major flow regimes observed were bubbly, slug and annular flow. Under certain conditions at high flow rates, a wispy-annular flow pattern was observed. The effects of mass velocity (0.2×10^6 - 2.4×10^6 lbm/hr-ft^2), inlet temperature (100, 150, 200°F), exit pressure (30, 100 psia), quality (x = -10 - +7 percent), purity (9, 40 PPM NaCl; 1-3 megohm-cm), length (L/D=30, 60, 90), diameter (0.094, 0.242 in.), and orientation (vertical and horizontal) on the flow regimes were studied. Flow regime maps on coordinates of mass velocity and quality are presented for these conditions.

Bubbly and slug flow occurred primarily in the subcooled region, while fully developed annular flow was reached at equilibrium qualities between 2 and 4 percent. The transitions between the different flows were shifted to regions of increased subcooling when velocity, pressure, and heat flux increased, and when inlet temperature decreased. Purity and geometry had little affect on the flow regime boundaries.

The shifting of the transitions is related to the agglomeration point, which is that point at which the bubbles so coalesce that slug flow is first observed. The agglomeration point depends on the point of incipient boiling, the number of bubbles in the flow, and the number of collisions per bubble. These latter quantities in turn depend on velocity, temperature, pressure, and heat flux.

The flow regime information obtained in this study should be of value in correlating and interpreting low pressure heat-transfer data. The flow regime data were found to be useful in explaining the effect of inlet temperature on burnout heat flux.

ACKNOWLEDGEMENTS

This study was supported by the National Magnet Laboratory of the Massachusetts Institute of Technology which is sponsored by the Solid State Sciences Division of the Air Force Office of Scientific Research. Machine computations were done on the IBM 7094 Computer located at the MIT Computation Center.

M. P. Fiori's studies at MIT have been supported by the United States Navy under the Junior Line Officer Advanced Scientific Educational Program (BURKE Program).

TABLE OF CONTENTS

LIST OF FIGURES

Fig.

NOMENCLATURE

A = heat transfer area (ft^2)

c_p = specific heat (Btu/lbm^oF)

D = diameter (in.)

G = mass velocity ($lbm/hr\text{-}ft^2$)

h = heat transfer coefficient ($Btu/hr\text{-}ft^{2o}F$)

h_e = enthalpy at exit (Btu/lbm)

h_f = enthalpy of saturated liquid (Btu/lbm)

h_{fg} = latent heat (Btu/lbm)

h_{in} = enthalpy at entrance to test section (Btu/lbm)

I = shunt voltage (mv)

k = thermal conductivity ($Btu/hr\text{-}ft^oF$)

L = length (in., ft)

P = pressure (psia)

P_e = pressure at exit of test section (psia)

q = rate of heat flow (Btu/hr)

q/A = heat flux ($Btu/hr\text{-}ft^2$)

$(q/A)_i$ = heat flux at incipient boiling ($Btu/hr\text{-}ft^2$)

$(q/A)_{cr}$ = critical heat flux ($Btu/hr\text{-}ft^2$)

R_I = oscilloscope internal impedance (ohms)

R_w = resistance between probe and tube wall (ohms)

R_v = variable resistance (ohms)

$T_{in,e}$ = water temperature at inlet or exit of tube (^oF)

T_b = water bulk temperature (^oF)

T_w = wall temperature (^oF)

T_s = saturation temperature (^oF)

V = voltage across test section (volts)

V_B = battery voltage (volts)

V_I = voltage across variable resistor (volts)

w = mass flow rate (lbm/hr)

x = quality

μ = viscosity (lbm/hr-ft)

Flow Regime Designations

B = ● = bubbly

BTS = ◐ = bubbly-to-slug transition

S = ○ = slug

STA = ◨ = first indication of slug-to-annular transition

STA = △ = slug-to-annular transition

A = ■ = annular

WA = ◔ = wispy annular

Chapter I

INTRODUCTION

1.1 Background of Problem

In recent years the interest in two-phase, gas-liquid flow has dramatically expanded as is indicated by the tremendous increase in the number of experiments and published papers in this field. If one examines the literature, one will find that a relatively large number of models have been proposed for analyzing and correlating experimental pressure-drop, heat-transfer, critical heat flux, and void-fraction data. These models frequently depend on the flow regimes (or flow patterns) which are geometric descriptions of the distribution of the liquid and gas phases within a channel. Gouse[1]* considers knowledge of the flow regime to be as important as knowing whether the flow is laminar or turbulent in single-phase flow.

Baker[2] showed that it was not practical to disregard the flow regimes in devising a two-phase pressure-drop correlation. Martinelli's[3] assumptions in his pressure-drop correlations tend to limit them to annular flow. Lavin and Young[4] propose boiling heat-transfer correlations for refrigerants, which are dependent on the flow regimes. Numerous models for the critical heat flux condition are based on the postulate of spray annular flow; however, there are some analyses which assume that fog flow is present.

*Numbers in parenthesis refer to References on p. 80.

It is apparent, then, that it is important to know the flow regime if one is to utilize an appropriate model; however, direct relationships between flow regimes and observables, i.e., pressure drop, heat-transfer coefficient, critical heat flux, and void fraction have not been clearly established.[5] It still appears, though, that flow regime observations will be helpful in reducing the complications of correlating the quantities of basic interest.

A survey of the literature indicates that flow regime studies have almost always been conducted under adiabatic conditions. However, exploratory studies have shown that flow patterns are considerably altered when there is heat addition, particularly in low pressure systems.[6] Comprehensive flow regime maps have been prepared at Dynatech[7][8] and Harwell[9] for high pressure boiling water systems. No similar study has been conducted at low pressures (below 100 psia).

Low pressure systems are receiving increased attention, particularly in the nuclear reactor and desalinization programs. In a recent study of critical heat fluxes at low pressure, Lopina[10] observed a pronounced effect of inlet temperature. For constant geometry, flow rate, and pressure level, the critical heat flux increased as the inlet temperature increased. This effect, which is contrary to what is observed at high pressures, appears to be related to the flow regimes. The phenomenon of

upstream boiling burnout in uniformly heated channels also appears to be related to flow regimes, in particular, the slug flow regime.

1.2 Flow Regimes

There have been various descriptions of flow regimes by different investigators. These classifications have often been quite arbitrary, and are also complicated by the fact that vertical and horizontal flows cause different regimes. Baker[2] described no less than seven different regimes in adiabatic two-phase, gas-liquid flow in horizontal pipes. Vohr[11] and Kepple and Tung[12] have presented complete bibliographies on studies of adiabatic flow patterns.

The flow regimes which may be encountered in flows in tubes with vertical upflow can be described in the order of increasing gas or vapor content. If very little gas or vapor is involved, the flow will be characterized by isolated vapor or gas bubbles dispersed rather uniformly in the continuous liquid phase. This is known as "bubbly flow". More bubbles appear with an increase of vapor or gas until the bubbles begin to touch one another and agglomerate. As more bubbles agglomerate, the gas begins to flow in long cylindrical, bullet-shaped bubbles. Between the bubbles are slugs of liquid and hence "slug flow". Further increase of the gas content destroys the stability of the bubbles, producing "churn flow" or "semi-annular flow" in which slugs of liquid separate adjacent gas

bubbles only temporarily. As the gas content continues to increase, the liquid flows on the wall as an annular film and the gas or vapor flows in the center of the tube. This geometry is called "annular flow". "Fog flow" or "dispersed flow" then follows where the gas or vapor phase occupies the entire tube but small drops of liquid are dispersed within it. This flow is also called "mist flow".

Other flow patterns which have been encountered are "froth flow", "spray annular flow" and "wispy annular flow". Froth flow is quite similar to bubbly flow except the bubbles are so numerous that the flow has a frothy appearance. Spray-annular flow is a combination of mist and annular flow. Some of the liquid flows in an annular film and some flows as small droplets in the vapor core. Wispy annular is similar to spray annular except the flow in the core consists of agglomerated liquid instead of small droplets.

There are very similar flow descriptions for horizontal flow. However, stratification is sometimes encountered in horizontal flow and several new regimes are introduced. "Plug flow" is similar to slug flow except that the bubbles move along the upper part of the channel or pipe. In "stratified flow" the liquid flows at the bottom, and gas or vapor at the top of the pipe.

These regimes appear to be quite well defined. However, for practical reasons it is desirable to minimize the number of regimes. Gouse[1] suggests that there are only four distinct flow patterns for vertical upflow: bubbly,

slug, annular, and mist; while all the others which have been observed are merely transitions from one to another.

The above flows were described for adiabatic conditions. In heated systems such clean geometric descriptions of the flow are not expected because of several characteristics not encountered under adiabatic conditions. Some of these characteristics are:

1) Vapor is continually formed along the tube. This creates a volume flow rate which continuously increases along the tube; thus the flow regimes would be expected to be different in different sections of thetube.

2) Bubbles may be generated and disturb the flow pattern.

In any case, the adiabatic flow regimes are a basis for interpreting and classifying the flow regimes with heat addition. The classification and both qualitative and semi-quantitative description of the flow patterns observed in this study are discussed in Section 2.3.3.

1.3 Flow Regime Detection

Numerous methods of studying flow regimes in heated systems have been developed. High-speed still and movie photography has been most popular. More exotic methods which have been used include isokinetic flow sampling, gamma or beta ray attenuation, and hot-wire anemometry. Each of these methods has drawbacks. Either there is too much data to analyze, as in the case of movies, or the methods are very complicated and expensive. The electri-

cal resistance probe which was developed by Solomon[13] specifically for flow regime detection, is an inexpensive, simple, and reliable device.

This probe measures the resistance between the centerline of the fluid flow and the tube wall. A bridge of liquid across the tube will cause a closed circuit, and gas or steam across the tube will result in an open circuit. Nassos[14] and Haberstroh[15] have successfully used this type of probe for adiabatic flow. Griffith[16] adapted this probe for a high pressure boiling water system and delineated the slug-to-annular transition. Dynatech[7][8] has recently been using this technique to map boiling water flow regimes at high pressures (500-1000 psia).

1.4 Scope of Research

A comprehensive study to examine boiling water flow regimes in tubes of small diameter at pressures below 100 psia was undertaken. A resistance probe described in detail in Section 2.2 was chosen as the primary means of flow regime detection; however, a visual section was also employed. The experimental program consisted of an investigation of the effects of velocity, inlet temperature, exit pressure, quality, (heat flux), purity, length, diameter, and orientation on the flow regimes. The first phase of the study was devoted to probe development and interpretation.

Chapter II

EXPERIMENTAL PROGRAM

2.1 Description of Apparatus

2.1.1 Hydraulic System

The experimental facility used was the low-pressure test loop located in the MIT Heat Transfer Laboratory. The basic apparatus was designed and constructed in 1961.[17]

A schematic of the loop is presented in Fig. 1. The pipings and fittings are made of brass and stainless steel for corrosion resistance. Rayon reinforced rubber hose is used where flexible connections are required. Distilled water is circulated by a bronze, two-stage, regenerative pump providing a discharge pressure of 260 psig at 3.6 gpm. The pump is driven through a flexible coupling by a 3-hp Allis-Chalmers induction motor. A Fulflo filter is installed at the pump inlet. Pressure fluctuations at the outlet of the pump are damped out by means of a 2.5-gal Greer accumulator charged with nitrogen to an initial pressure of 40 psig. This accumulator contains a flexible bladder-type separator which prevents the nitrogen from being absorbed by the system water. After the accumulator, the flow splits into the by-pass line and the test-section line.

In the test-section line, fluid flows through a Fischer-Porter flowrator followed by a preheater, thence through a Hoke metering valve and the test section, after which it merges with fluid from the by-pass line. The

flow then goes through the heat exchanger and returns to the pump. The preheater consists of four Chromalox heaters of approximately 6 kw each. Three of these are controlled simply with "off-on" switches while the fourth can provide a continuous range from 0 to 6 kw by means of a bank of two variacs mounted on the test bench. Quick-action Jamesbury ball valves are installed before the inlet to the flowrator and after the exit from the test section. This permits quick isolation of the test section to minimize fluid loss when conducting burnout tests. The exit valve is also used to adjust the test-section pressure.

Flow through the by-pass line is controlled by a ball valve on each side of which there is a 300-psig pressure gage. Pump operating pressure, and hence the pressure upstream of the test section, is controlled by this valve.

The heat exchanger is a counterflow type with system water flowing in the inner tube and city water in the outer annulus. Except at very high power levels, the heat exchanger maintained a constant pump inlet temperature. A Fulflo filter is installed on the city water line to reduce scale formation in the exchanger.

The distilled water was de-ionized continuously, except during contamination studies, by passing a portion of the flow through four mixed-bed resin demineralizer cartridges installed in a Barnstead- "Bantam" demineralizer unit. A 4.7-gal degassing tank is provided with five electrical heaters (3-200 vac and 2-110 vac). This tank also

serves as a surge tank. A 15-gal stainless-steel storage tank for filling the system is mounted directly above the degassing tank and can be filled with distilled water from standard 5-gal bottles with a small Hypro pump.

2.1.2 Power Supply

Test-section electrical power is provided by two 36-kw dc generators connected in series. Each generator is rated at 12 volts and 3000 amperes. The power control console permits coarse or fine control from 0 to 24 volts. A water-cooled shunt installed in parallel with the test section protects the generators against the shock of the sudden open circuit which occurs at burnout. Power is transmitted from the main bus to the test section by water-cooled power leads. In the present tests, the downstream or exit power lead was at ground potential. Rubber hose connected both inlet and exit chamber plenums to the main loop in order to electrically isolate the test section. The exit of the test section was then separately grounded (see schematic of test section, Fig. 2).

2.1.3 Instrumentation

All temperatures were measured by copper-constantan thermocouples made from 30-gauge Leeds and Northrup duplex wire. The test-section inlet temperature was measured by a thermocouple directly in the fluid stream, upstream of the Hoke metering valve. The thermocouple was introduced at this location through a Conax fitting equipped with a lava sealant.

All pressures were read on Bourdon-type gages located as shown in Fig. 1. The test-section inlet and exit pressures were measured with Helicoid 8-1/2 in. gages of 200 psig and 100 psig, respectively. Both are specified to an accuracy of $\pm$0.25% of full scale.

A variety of metering tubes and floats, which could be installed interchangeably in the basic Fischer-Porter flowmeter housing, provided measurement of the test-section flow from 1.5 to 4000 lbm/hr.

The voltage drop across the test section was read directly on a Weston multiple-range dc voltmeter with a specified accuracy of $\pm$ 1/2 percent. The current flow was determined by using the Minneapolis-Honeywell, Brown recorder to measure the voltage drop across a calibrated shunt (60.17 amp/mv) in series with the test section.

The details of the resistance probe are discussed in Section 2.2. Polaroid cameras were used for the photographic study. The camera settings and procedures are discussed in Appendix B.

2.1.4 Operating Procedures

After the test section was installed, the loop and degassing tank were filled with distilled water from the supply tank. The water in the degassing tank was then brought to a boil while the loop water was circulated with the heat-exchanger coolant off. Degassing was accomplished by by-passing a portion of the loop water into the top of the vigorously boiling degassing tank. This was continued

until the temperature of the loop rose to approximately 180°F. A standard Winkler analysis described in Ref. 17 indicated that this method of degassing reduced the air content to less than 0.1 cc air/liter. After completing degassing, the loop water was adjusted to the desired inlet temperature and the desired pressures were set. A pressure of from 210 psig to 260 psig was maintained at all times on the upstream side of the Hoke metering valve to prevent system-induced instabilities. The generators were then started and allowed to warm up.

Nine burnout tests were made in order to have reliable critical heat flux data for conditions similar to the planned flow regime studies. This knowledge aided in avoiding burnout of the probe test sections. Power was applied to the test section in small increments while maintaining a constant flow rate and inlet temperature. The test-section flow rate, shunt voltage (test-section current), inlet temperature, and exit pressure were recorded for each voltage setting. The critical or burnout heat flux was defined to be that heat flux which caused physical failure of the test section. After commencing flow regime studies, it was seen that the area of interest was usually far removed from $(q/A)_{cr}$. Consequently no further burnout studies were made. Appendix A contains a tabulation of the burnout points.

The same data were recorded for the flow regime runs. A run consisted of taking data at a particular mass flow rate for a given set of conditions, i.e. D, L/D, T_i, P_e.

As the power was increased, various responses on the oscilloscope indicated the type of flow (see Probe Interpretation, Section 2.3). Water purity was checked by means of a Barnstead Purity Meter (0.1 - 18 megohm-cm) or an Industrial Instruments Solu-Bridge Meter (0 - 30 PPM NaCl).

2.2 Resistance Probe and Test Section

2.2.1 Principle of Operation

The resistance probe was used to determine the flow regime at the exit of the test section. The probe is a wire placed in the center of the tube as shown in Fig. 2. This wire is covered by teflon sleeving except for the tip of the wire. The circuit diagram for the probe is shown in Fig. 3a. When there is a bridge of water across the tube at the test-section exit, there is essentially a closed circuit between the probe and the tube wall. This results in a maximum voltage across resistor R_V which is measured by an oscilloscope. On the other hand, steam passing between the probe and the wall resembles an open circuit giving a voltage reading across R_V near zero.

2.2.2 Probe Integration with Test Section

Two types of test sections were used for this study. The first type was used for preliminary burnout studies. The second type incorporated the resistance probe and a sight section. The sight section was not always used because the rubber gasket would not hold for exit pressures above 40 psig. The heated sections were made of standard

304 stainless tubes. The burnout test sections and the first probe test section had an 0.242-in. i.d. and 0.3125-in. o.d. while the second probe test section had an i.d. of 0.094 in. and o.d. of 0.120 in. The details of the two test sections are shown in Fig. 2.

In the burnout test section, 3/4-in. brass bushings were silver-soldered to the stainless steel tube to form the power connections upstream and downstream. A pressure tap was installed in each exit bushing with a No. 80, 0.0135-in. diameter hole drilled through the tube wall. The pressure tap was placed here rather than in the exit plenum chamber because of the choking phenomena whereby the plenum pressure is lower than the exit pressure.[10]

The probe test section had pressure taps located at both the inlet and exit. The exit section was modified to include the probe and pyrex sight section. The inside diameter of the glass tubing was equal to the outside diameter of the test section. This caused a slight expansion at the entrance to the visual section.

The brass supporting structure for the probe, pressure tap, and sight section also served as the exit power connection. The pressure tap is similar to the previous one described.

The probe was fabricated from 0.035-in. diameter tempered stainless-steel spring wire for the 0.242-in. diameter tube and from 0.015-in. wire for the 0.094-in. diameter tube. Teflon spaghetti was slipped over this wire and

stretched until the teflon set snugly on the wire. The final probe diameters were 0.060 in. and 0.031 in. Even the small diameter probe had adequate stiffness to prevent vibration which could create spurious signals.

The straight probe was pushed into the test section from the packing gland side until it touched the opposite wall. The tip was then carefully bent and the teflon was forced around the wire until only a 1/4 in. of probe tip was bare.

The teflon acts as an insulation between the probe and the tube wall. More important, since teflon is not wetted by water, there is no chance of a short-circuit between the exposed end of the wire and the tube wall. The drying time of the teflon after passage of a slug of liquid is extremely short, less than 10^{-3} seconds as observed with an oscilloscope.(15)

2.2.3 Probe Sensitivity

A schematic diagram of the probe circuit is shown in Fig. 3a. It can be shown that the voltage reading, V_I, is related to the resistance of the water-steam mixture in the test section, R_w, by the equation

$$V_I = \frac{V_B}{R_w\left(\frac{1}{R_v} + \frac{1}{R_I}\right) + 1} \qquad (1)$$

Furthermore, it can be shown that the maximum sensitivity, defined by a maximum in $\left(\frac{\partial V_I}{\partial R_w}\right)$ is obtained when

$$\frac{1}{R_w} = \frac{1}{R_v} + \frac{1}{R_I} \qquad (2)$$

At this maximum sensitivity, the instrument voltage, V_I, is related to the battery voltage, V_B, by the equation

$$V_I = \frac{V_B}{2} . \qquad (3)$$

The dependence of V_I on R_w, for $V_B = 6$ volts and $R_I = 10^6$ ohms, is indicated in Fig. 3b. The lowest value of R_w occurs when saturated liquid is flowing in the test section. During the course of the experiments, R_w for saturated liquid was found to vary between 10^5 and 2×10^6 ohms. For the lower limit of $R_w = 10^5$ ohms, it can be seen that for $R_v = 10^5$ ohms, the maximum sensitivity will occur in the liquid region. For $R_v = \infty$ the maximum sensitivity will occur at a much higher R_w corresponding to a flow pattern with a higher void fraction. Consequently, by adjusting R_v, the maximum sensitivity can be chosen to correspond to a flow regime boundary. However, since these boundaries are not known in advance, it is desirable to maintain R_v at a fixed value for each run. It was found most convenient to adjust R_v so that maximum sensitivity was obtained in the bubbly region. This could not always be achieved due to the restriction imposed by the internal resistance of the oscilloscope. This, however, did not affect the results to any noticeable degree since the variable of interest was the shape rather than the value of V_I.

2.3 Probe Interpretation

The output of the probe for typical runs is described below. Throughout the interpretation phase of the experiment, Polaroid photos were simultaneously taken of the exit flow and of the oscilloscope trace.

2.3.1 Velocity Effect on Probe Signal Amplitude

With stationary water in the test section, a large signal was obtained. When the pump was started and water began to flow, the signal decreased by one to two volts. As the water velocity increased, the voltage decreased, although the decrease was much less than that observed at startup. Other experimenters[15] also observed this effect and speculated that this is an "electrokinetic" effect, associated with the charge-carrying capacity of the water.

2.3.2 Temperature Effect on Probe Signal Amplitude

When the power was applied to the test section, the bulk fluid temperature increased and the voltage trace increased. This voltage increased to a maximum as the saturation temperature was reached. This was expected since the conductivity of the water increases with temperature, causing a greater voltage drop across the variable resistor, R_V. To insure that this effect was only due to temperature, power was shut off and the water temperature was increased by means of the preheaters. The same effect was observed.

2.3.3 Flow Regimes Related to Probe Signal

The number of distinct flow regimes of two phase flow was shown to be somewhat arbitrary. Four main flow patterns were recognized in the present experiments: bubbly, slug, annular, and wispy annular flow. The physical or geometric description of the observed flow patterns is very similar to that given in Section 1.2.

Bubbly flow is characterized by a continuous liquid phase with small vapor bubbles dispersed somewhat uniformly throughout the tube. The characteristic bullet-shaped bubbles of slug flow could not be identified under the present high heat flux conditions. Slug flow was recognized whenever large, irregular bubbles, whose size was on the order of the diameter of the tube had somewhat continuous slugs of water between them. Annular flow consisted of a thin film of liquid, usually quite turbulent, flowing along the wall, while vapor and fine droplets flowed in the center of the tube. This has often been called spray-annular flow, but for the purposes of this report, annular will be used. The character of the core flow was inferred from the charge carrying spray effect which is discussed in Sec. 2.3.4. Wispy annular flow was characterized by a continuously increasing void fraction without the distinct characteristics of the above three flows.

Since the classification of these flow regimes is rather qualitative, different individuals may interpret the flows differently. The data in Figs. 4, 5, and 6 were chosen so as to indicate the semi-quantitative definitions of the flows which were used throughout this study. Figure 7 presents a summary of the probe traces for the various flow patterns.

Bubbly Flow In Photo I in Fig. 4, a 2.8-volt signal with very small fluctuations is observed. These small fluctuations are due to bubbles which can be seen in the sight

section. Figure 7a shows the schematic of the oscilloscope trace for bubbly flow. Incipient boiling could not be detected by the probe due to the small amount of vapor generation. It could not be detected with the sight section either, because these bubbles recondensed in the subcooled bulk flow before visual observation could be made.

Bubbly-to-Slug Transition The transition from bubbly to slug (BTS) flow was first defined when the small pips previously seen in bubbly flow became large enough to produce a 1.0 - 1.5-volt deflection. Photo II graphically shows a large bubble just leaving the heated section. This bubble caused a 1.3-volt deflection on the scope trace. This transition, schematically shown in Fig. 7b, was well defined and reproducible.

Slug Flow Slug flow was considered to be present when the probe signal alternated between all-liquid and all-vapor levels. In Photo III it is noted that clean bubbles and slugs, of the variety found in adiabatic flow, do not exist. The bubble is like a vapor void without a definite head or tail, and the slugs have small bubbles dispersed throughout. At high flow rates, the slug trace was somewhat different, as seen in Photo IV. The frequency of the full deflection is increased dramatically and the flow appears to be very agitated. Figures 7c and 7d show the first full slug and slug flow, respectively.

Slug-to-Annular Transition The transition criterion for the slug to annular (STA) was more subjective than the

other criteria. From Fig. 7d it is seen that for slug flow, the voltage deflections average out between $(V_I)_{max}$ and 0. In Fig. 7e it appears that the slugs are thinner and a larger percentage of vapor is passing the probe. The STA transition was defined when the voltage deflections appeared to rise from 0 volts up, rather than from $(V_I)_{max}$ down. An example of this flow is seen in Photo V. It is noted that it would be very difficult to distinguish this flow from annular flow, particularly at high G, using the sight section alone. As test-section power increases further (Photo VI, Fig. 7f), the voltage trace is similar to that of the initial description of the STA transition except that the peak voltages are not full deflections. This flow is still the transitional flow from slug to annular. Physically, it appears as if most of the tube consists of annular flow, but much of the liquid transport is still in the very rapidly moving slugs.

Annular Flow With greater power, the voltage deflections become smaller, thus indicating that the annular flow region is being approached. Annular flow was defined to be that flow which would give an average deflection no greater than 0.5 volts (Fig. 7g). This definition did allow larger deflections to occur, but the frequency of these large deflections was greatly reduced. At low velocity annular flow was well defined since the voltage was practically zero (Photo VII). Photo VIII is another example of annular flow. The increased velocity of the vapor core caused large wave-

like motions on the surface of the annular film. These waves appeared as large deflections on the oscilloscope. As G was increased, these waves increased in frequency and the film had a milky appearance, probably due to the increased entrainment and deposition of droplets. Very little could have been said about the interior flow, i.e. waves, if only photography had been used in this study.

Wispy Annular Under certain conditions, i.e. $T_{in} = 200^{o}F$, $P = 20\text{-}30$ psia, $G = 1.6 - 2.0 \times 10^{6}$ lbm/hr-ft^2, a variation of the above flow regimes was noted. As power was increased beyond bubbly flow, a strong bubbly trace travelled downward from $(V_I)_{max}$ to 0 volts. Slug flow did not appear and in its place was a flow which can be called wispy annular[9] or froth[8]. The behavior of the trace is schematically shown in Figs. 7h, 7i, and 7j and in the corresponding Photos IX, X, and XI. As the void fraction is increased, the resistance between probe and wall becomes greater until annular flow is reached. It would be possible to describe many flow patterns in this high-velocity transition between bubbly and annular flow. Froth flow would probably be a more appropriate description of the beginning of this transition, while wispy annular could describe the latter part of the transition. Since the probe indicated that the transition was quite homogeneous throughout, it appears that a single classification is adequate.

2.3.4 Charge Carrying Spray Effect

Photo XII again shows annular flow, but the oscilloscope trace is radically different in that negative traces up to one volt are seen. This type of trace was not observed in high pressure studies[16,8] and initially caused quite a bit of trouble in interpretation. With the probe circuit battery removed and the oscilloscope connected directly across the probe, a fluctuating negative voltage was still observed. The magnitude and frequency of this fluctuation increased as the flow rate was increased, even though no voltage source was present. A possible pickup effect on the probe from the voltage across the test tube was discounted because the generator output voltage did not have such large fluctuations.

The explanation of this negative voltage effect is believed to be as follows. As annular flow is approached, small droplets of water are torn away from the liquid film and are transported as a spray in the core. By some physical effect these droplets become negatively charged upon detaching from the bulk flow, thus leaving the film positively charged. The droplets travel down the tube and rejoin the film and lose their charge, escape through the exit and lose their charge in the loop, or deposit their charge on the probe. This last possibility appears to be the source of the negative voltage observed on the scope. Professor D. P. Keily[18] has observed such effects with aerosol-type flows and indicated that voltages up to

several volts could be observed if there were enough droplets. The mechanism that causes the detached particle to have a negative charge has not been identified. It appears that this effect is quite important and should receive more attention. Vonnegut, et al.[19] indicate that such charged water droplets are produced naturally in clouds and thunderstorms and as spray from lakes and oceans.

This negatively-charged droplet theory is substantiated by several observations. When the water was particularly pure, i.e. 3 megohm-cm and above, this effect was quite strong. However, after adding salt to the water (30-40 PPM), the negative voltage was not observed. The sketches k and l in Fig. 7 show this purity effect.

The more conductive water allows more of the negatively charged particles to transfer their charge to the liquid film rather than depositing it on the probe. This also explains why the Dynatech workers, who used a similar probe, did not observe this effect. They were operating at 500 and 1000 psia and had a correspondingly higher temperature level. The conductivity of water increases greatly as the temperature increases; for example, the conductivity of pure water due to ionization is about a 1000 times greater at 546°F than at 77°F.[20] Consequently, this conductive water allowed the negative charge to leak into the liquid film before hitting the probe. With this theory, it would be expected that the negative voltage would increase with increased mass flow rate. This effect was also observed, as stated earlier.

Several methods were attempted to eliminate this effect electronically by using a higher battery voltage, and by using an ac high-frequency voltage source. The first method reduced the relative voltage of the effect but did not eliminate it. By means of filter circuits and high frequency ac, it was hoped to eliminate the spurious negative charge and retain only the desired signals. However, the filters and bias circuits also removed the desired fluctuations. With experience it was found that proper interpretations of the flows could be made even though the negative voltage was present.

2.3.5 Reproducibility and Reliability of Probe Output

About a dozen runs under various conditions were repeated for a second time. When these runs were compared to the original ones, it was seen that they were almost identical. It was concluded that any run could be repeated with the expectancy of getting very similar results.

The sight section observations were quite helpful in interpreting the probe traces. However, when the bulk temperature was moderately subcooled, the vapor condensed rapidly in the sight section and it was necessary to look into the exit of the heated section to get an accurate visual indication of the flow pattern. When the void fraction was large, the flow was usually so disturbed that it was difficult to visualize the flow pattern. In both of these situations the probe was able to distinguish the important features of the flow.

2.4 Test Program

After the probe calibration and interpretation runs were completed, the actual flow-regime investigations were started. The following table lists all the sets of runs completed in this experimental program.

All the data are presented on flow regime maps. The coordinates of mass velocity (G) and mass quality (x) were chosen because it appeared that they were best suited in presenting the various effects studied. In addition, they are usually the most convenient for engineering applications. Researchers in adiabatic two-phase flow frequently make use of volume flow rate and volume quality coordinates. They could not be used for this study since nonequilibrium effects dominated and these quantities cannot be calculated. Several runs are also presented in terms of heat flux and quality to demonstrate a particular effect.

Due to the manner in which the loop operates, it was difficult to control the exit pressure very accurately. Consequently, pressure comparisons were made at low pressures where the exit pressure varied from 20-35 psia and at high pressures between 90-100 psia. These small pressure differences did not affect the results to any appreciable degree, in comparison to the effects due to the large difference between high and low pressures.

2.5 Data Reduction

All data were reduced by machine computation. The IBM 7094 Computer at the MIT Computation Center was used. The

Table 1

Set	L/D	D (in.)	T_i °F	P_e (psia)	G x 10^{-6} ($\frac{lbm}{ft^2-hr}$)	Water Purity Megohm-cm (or PPM)	Fig.
1	60	0.242	100	~20-30	0.4-2.0	9 PPM	8
2	60	0.242	100	~20-30	0.8-2.0	0.48 megohm-cm	9
3	60	0.242	100	~20-30	0.2-2.4	2.5	10
4	60	0.242	150	~20-30	0.2-2.4	~ 2	11
5	60	0.242	200	~20-30	0.2-2.4	~2.5	12
6	60	0.242	100	~100	0.4-2.4	Water was checked at least three times in every set and found to be between 1.-3.0 megohm-cm.	13
7	60	0.242	200	~100	0.4-2.4		14
8	30	0.242	100	~ 30	0.2-1.6(B.O.)		15
9	90	0.242	100	~30	0.2-2.4		16
10	90	0.242	100	~100	0.4-2.0		17
11	60	0.094	100	~30	0.4-2.4		18
12	60	0.094	200	~30	0.4-2.4		19
All previous sets were horizontal, No. 13 is vertical							
13	60	0.242	100	~30	0.2-2.0		20

program is described in Appendix C. The heat flux was determined by the formula

$$(q/A) = \frac{EI}{\pi DL} \tag{4}$$

The equilibrium exit quality is given by

$$x = \frac{q/w + h_i - h_f}{h_{fg}} \tag{5}$$

Chapter III

PRESENTATION AND DISCUSSION OF RESULTS

3.1 Effects of Variables on Flow Regimes

Experiments were conducted to investigate the effects of velocity, inlet temperature, exit pressure, quality, purity, length, diameter and orientation on the flow regime boundaries. Figures 8 through 20 present all of the flow regime data in terms of mass velocity versus quality. In accordance with the discussion in Chapter II, the following flow patterns were identified: bubbly, bubbly-to-slug transition, slug, slug-to-annular transition, annular, and wispy annular.

It is seen in all the maps that the bubbly and slug flows occurred primarily in the subcooled region, while full annular flow was developed at 2 to 4 percent quality. The two-phase flow is therefore in a highly nonequilibrium state and a considerable volume of vapor coexists with the subcooled liquid.

From all the maps, it is observed that the transitions occur at greater subcooling or lower quality as the velocity of the flow is increased.

The influence of the remaining variables on the flow regime boundaries can best be illustrated by composite plots. At this point it is desirable to consider only the major flow regimes. It is noted that the transition regions occasionally cover a broad enough range of quality so that they could possibly be classified as flow regimes. However, practical considerations dictate that the number of regimes

be kept to a minimum. Boundary lines were drawn through the center of the transition regions and these lines were then transferred to the appropriate composite plots. These plots are presented in Figs. 21 through 27.

Figures 21 and 22 indicate that the transitions occur at higher quality as the inlet temperature is increased from 100 to 200°F. The transition bands for T_i = 200°F are much narrower than those for T_i = 100°F (Figs. 10 and 12). In addition, it is noted that slug flow was not observed above G = 1.2 x 10^6 lbm/hr-ft^2 with the higher inlet temperature. These latter effects were also observed for the smaller diameter test section (Fig. 19), but were not observed at higher pressure (Fig. 14).

At T_i = 100°F, at 30 and 100 psia, particularly at high G, the transition from slug to annular flow was noticeably more violent causing the test section, the connecting rubber hoses, and piping to vibrate considerably. While testing the L/D = 30 tube, violent vibrations were also observed at this transition. This tube burned out in this region in spite of the fact that the heat flux was not near the critical flux reported by Lopina.[10]

Pressure had a considerable effect on the location of the flow regime boundaries. Increasing the pressure from 30 psia to 100 psia shifted the flow regimes to substantially lower quality. Figure 23 shows this pressure effect at T_i = 100 and 200°F.

In order to eliminate the negative voltage problem previously described, salt was added to increase the conduc-

tivity of the water. The effect of this dissolved impurity on the flow regimes is illustrated in Fig. 24. The BTS transition for very pure water (2.5 megohm-cm) occurs at slightly higher quality than the transition for the 1 and 9 PPM water. There was no discernible effect in the STA transition. Conductivity variations between 1 and 3 megohm-cm produced no noticeable shift in the flow regimes.

Length-to-diameter ratios of 30, 60 and 90 were examined. From Fig. 25, it is seen that the flow regimes are quite similar, although for an L/D = 30 the transitions are at slightly lower quality.

For the same T_i there was no discernable difference in the flow regime maps for the two diameters (Fig. 26).

In Fig. 27 it is seen that the transition lines have the same general shape for the horizontal and vertical test sections. There is a slight shift to lower quality for the vertical section. At velocities below 0.4×10^6 lbm/hr-ft^2, slight stratification was visually observed for the bubbly and BTS transitions. Since the vertical test section showed only a minor flow regime variation from the horizontal section, it is evident that this stratification did not affect the probe output at the particular position, i.e. center, that the probe was in. A modification of the probe design, whereby the probe could be moved radially across the tube during operation, would allow examination of the flow very close to the walls and thus would detect any stratification.

3.2 Explanation of Results

The various effects noted above appear to be very closely related to incipient boiling, heat flux, and turbulence of the flow. To explain this relationship, the requirements for the transition to slug flow are first examined.

Radovich and Moissis[21] have shown that the frequency of bubble collisions is very high in two-phase bubbly flow. A relatively small number of these collisions results in coalescence. As more bubbles coalesce, the bubbles increase in size to such an extent that slug flow is observed. The time that it takes to cause the first identifiable existence of slug flow has been called the agglomeration time. The agglomeration time is thus determined by the collision frequency and the probability of coalescence per collision. The latter quantity was found to be strongly dependent on the purity of the liquid. Since the liquid used in this study was maintained at relatively constant purity for most of the experiments, the agglomeration time depended primarily on the collision frequency. A decrease in the agglomeration time would mean a shifting of the BTS transition to lower quality. This could be accomplished by increasing the number of bubbles and by causing greater turbulence in the flow.

The requirements for incipient nucleation in a forced-convection surface-boiling system have been considered in detail by Bergles and Rohsenow.[22] When their correlation

was applied to the present conditions (Appendix D), it was found that incipient boiling occurred at greater subcooling as G increased, T_i decreased, and P_e increased. Furthermore, it can be seen from Figs. 28 to 31 that the heat flux level increases as G increases, T_i decreases, and P_e increases. As the heat flux increases there is an increase in the bubble population. Bowring[23] has concluded that as heat flux and velocity increase, there is an increase in the subcooling at which detatchment of the bubbles from the heated surface occurs. This is due primarily to a general increase in turbulent mixing under these conditions. This enhanced mixing should promote the agglomeration of bubbles.

Thus, on the basis of incipient boiling, heat flux, and mixing considerations, one would expect a shift in the BTS transition to greater subcooling as G increases, T_i decreases, and P_e increases. These trends are observed in the present data, as was discussed in the preceding section. Since the heat flux level increases as the tube length decreases, the shifting of the BTS transition to greater subcooling as length is decreased is also accounted for.

Regarding the other transitions, it is reasonable to expect that if the BTS transition occurs at lower quality, the STA transition should also occur at lower quality. In particular, the increased bubble agitation at the higher heat fluxes would be expected to break up the slugs, thereby promoting annular flow.

The limited occurrance of wispy annular flow can be related to the above arguments. It is recalled that this regime occurred only for high inlet temperature and low pressure. Under these conditions the heat flux level is low and there are fewer bubbles and also less tendency for the bubbles to agglomerate into slugs. The core flow remains bubbly or forthy in appearance until the void fraction is so high that the spray annular configuration is reached. In general the wispy annular regime is only observed at high velocity where the short transit times are less condusive to formation of slug flow.

At this point it is worth mentioning that Radovcich and Moissis predicted that the BTS transition would be much more rapid for pure water. As discussed in the preceding section, the present tests indicated that this transition for the demineralized water occurred at about the same quality as that for the water with dissolved salt. Their observation was for adiabatic flow; thus, with heat addition the other mechanisms appear to overshadow the impurity effect.

3.3 Interpretation of Critical Heat Flux Data by Means of Flow Regimes

The present flow regime observations should be useful in interpreting heat transfer and pressure drop data for boiling water at low pressures. As an example of the application of the present data, one of the important effects in bulk boiling burnout will be considered.

Recent studies of bulk boiling at low pressure have confirmed that the critical condition coincides with the disappearance of the liquid film from the heated surface.[24] The film can be depleted by evaporation and entrainment, or it can be disrupted by bubble nucleation. In addition to these local effects it appears that unstable upstream flow patterns can produce a disruption of the annular film further downstream.

Lopina[10] found that the burnout heat flux increased as the inlet temperature increased. Typical data illustrating this effect are plotted in Fig. 33. The flow regimes for these conditions are superimposed on the operating lines.

First consider operation at high inlet temperature as shown in Fig. 33. The majority of the tube is in annular flow with only moderate increases in heat flux. The slug flow region of the tube becomes increasingly violent, but also moves toward the inlet, as the heat flux is increased. This unstable slug flow region should have little effect on the critical heat flux, which for these flow conditions is probably caused by nucleation-induced breakup of the film. Now, as the inlet temperature is decreased, the slug flow region remains in closer proximity to the exit of the tube and the disturbance created within this region would be expected to propagate downstream and affect the film at its thinnest point, which is at the exit of the tube. A significant reduction in the critical heat flux is thus

observed as the inlet temperature is increased.

With short test sections the operating region will lie in the vicinity of zero quality. In this case the unstable slug flow regime is at the exit to the test section and relatively low burnout fluxes, noted in the present L/D = 30 tests, for example, would be expected.

Chapter IV

CONCLUSIONS

4.1 Conclusions

The conclusions of this investigation can be summarized as follows:

1) The electrical resistance probe is exceptionally well suited for flow regime studies. It is simple, inexpensive, and provides reliable and consistent results. For low pressure studies, where nonequilibrium effects dominate, the probe is more reliable than an exit sight section.

2) The interesting phenomenon of the spray particles carrying a negative charge has been observed. The cause of this effect is not yet known, but various researchers are investigating the problem. Although it influenced the probe output under certain conditions, it did not inhibit the flow regime analysis.

3) Flow regime observations were made for low pressure water over a wide range of flow conditions. The major flow regimes observed were bubbly, slug, annular, and wispy annular flow. The flow regime maps show that bubbly, transition to slug, slug, and transition to annular flow occur in the subcooled region under nonequilibrium conditions while a fully developed annular flow exists by the time 2-4 percent quality is reached.

4) The observed effects of the parameters on the flow regimes are summarized in the table below.

Table II

Parameter	Direction of Change in Parameter	Direction of Shift of Flow Regime Boundaries
Mass Velocity	Increase	towards greater subcooling
Inlet Temperature	Increase	towards less subcooling
Pressure	Increase	towards greater subcooling
Purity	Decreased	negligible change
Length	Increased	slight change towards less subcooling
Diameter	Decreased	negligible change
Orientation	Horizontal to vertical	negligible change

5) The influence of velocity, temperature, pressure and length on the flow regime boundaries can be explained in terms of incipient boiling, heat flux, and turbulent mixing considerations.

6) The present observations were applied to bulk boiling burnout data. It was found that the effect of inlet temperature on burnout can be related to unstable upstream flow patterns.

APPENDIX

APPENDIX A

Burnout Data

Date: 19 and 21 July 1965

T_i = 100°F

i.d. = 0.242 in.

L/D = 60

Run	P_e (psia)	$G \times 10^{-6}$ (lbm/hr-ft^2)	x percent	$(q/A)_{cr} \times 10^{-6}$ (Btu/hr-ft^2)
1	27.0	0.5	33.0	0.962
2	28.0	0.4	37.0	0.843
3	43.5	0.8	30.6	1.51
4	34.0	0.8	19.0	1.12
5	37.5	1.2	11.6	1.36
6	36.0	1.2	10.9	1.32
7	51.0	1.6	10.76	1.81
8	45.0	1.6	8.35	1.64
9	48.0	2.0	4.15	1.71

APPENDIX B

Photographic Procedures

For the photographic study, simultaneous pictures were taken of the oscilloscope trace and of the exit flow in the glass sight section. This was accomplished by shooting both pictures manually at the same time at the desired flow conditions.

The Polaroid Oscilloscope Camera for the Hewlett-Packard Company Model 130B/BR Oscilloscope was used. The film was Polaroid ASA 3000 film and the camera settings were f 2.8 and speed of 1/30 sec.

The sight section was normally illuminated by a General Radio Co. Strobotac. The Strobotac was always off when actually taking photos.

For the sight section photos, Polaroid ASA 200 Film was used in order to obtain better quality pictures. A General Radio Co. Type 1530-A Microflash was used to illuminate the exit test section. The 2-microsecond light pulse effectively stopped the motion of the flow in the sight section. Various backgrounds for the sight section were tried with black velvet giving the best results. The Polaroid camera was mounted on a tripod and the +2 and +4 Polaroid close-up lenses were used. The camera settings were f.8 and 1/30 sec.

Below is a sketch of the lighting setup viewed from above. The microflash was approximately 12 inches below the test section and was inclined so that the light was pointed directly at the sight section.

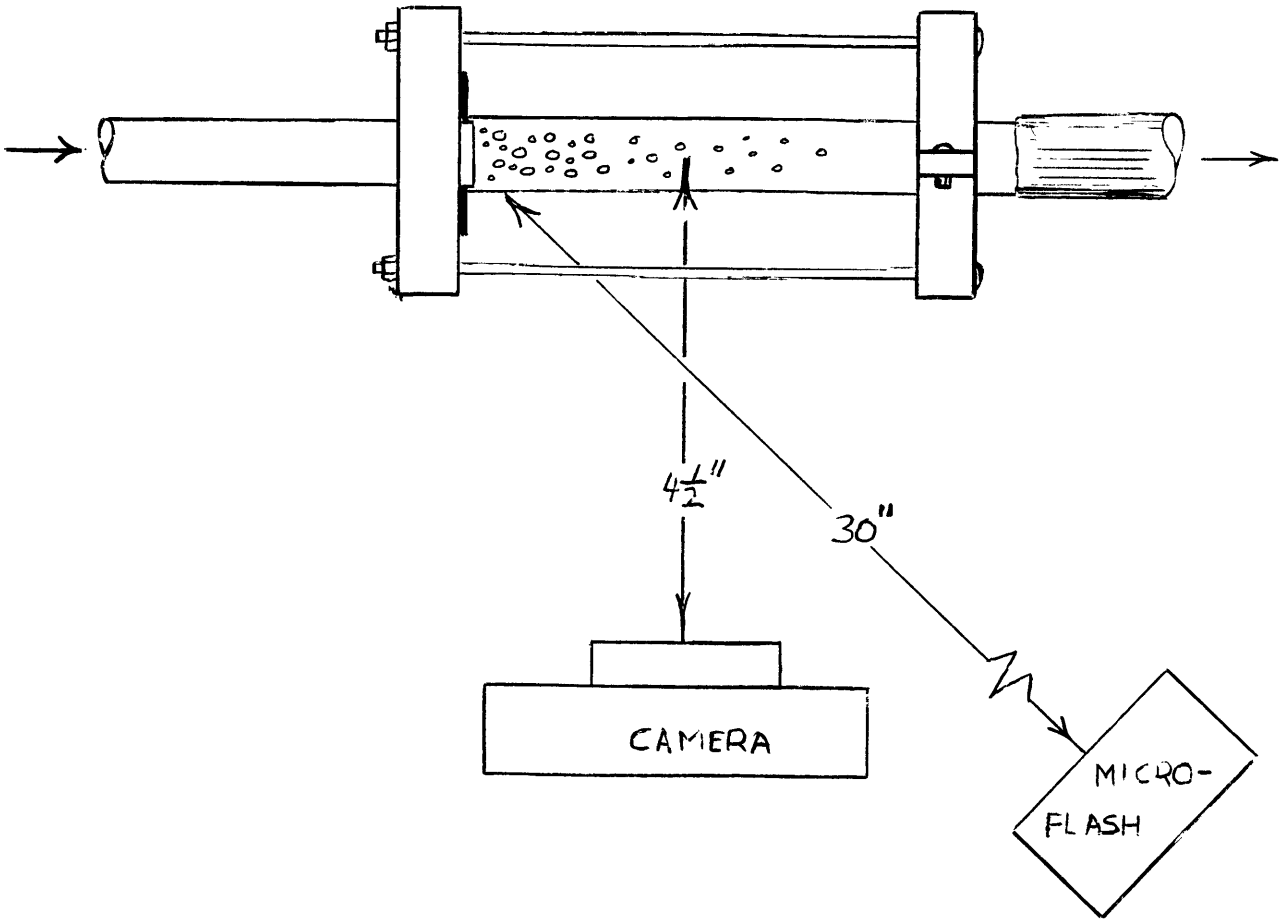
4½"
30"
CAMERA
MICRO-
FLASH

APPENDIX C

Computer Program for Data Reduction

The experimental data obtained was reduced in accordance with the equations in Section 2.5 by a program written in FORTRAN and run on the MIT Computation Center IBM 7094 Computer.

The input data consisted of the run identification number, the exit pressure, voltage across the test section, shunt voltage (current through test section), enthalpy of the incoming fluid, and the mass flow rate.

The program calculated the rate of heat transfer, heat flux, rate of heat transfer per pound mass of water, enthalpy of saturated liquid, latent heat, and quality.

Below is a list of the variables as used in the program and their physical counterpart.

PROGRAM VARIABLE	PHYSICAL COUNTERPART
I, J, K	Numeral run identification numbers
P EXIT	P_e exit - the pressure at the test section (psia)
E	V - voltage across test section (volts)
CUR	I - shunt voltage (mv)
HIN	h_{in} - enthalpy of incoming subcooled water
W	w - mass flow rate (lb/hr)
A	A - heat transfer area (Changed this value for each L/D and D) (ft^2)
HADDED	q - rate of heat flow (Btu/hr)
HTFLUX	q/A - heat flux (Btu/hr-ft^2)

BTULBM	q/w - rate of heat flow per lbm of water (Btu/hr-lbm)
ENFPX	h_{fe} - enthalpy of saturated liquid at exit (Btu/lbm)
ENFGPX	h_{fg_e} - latent heat at exit (Btu/lbm)
X	x - quality

The enthalpy of saturated liquid (h_f) as a function of pressure was obtained by Todreas[25] by a power series fit of the Keenan and Keyes' values. For P < 200 psia

$$h_f(P) = \sum_{i=o}^{9} a_i P^i$$

where

$a_o = 1.1222734(10^2)$ $\quad$ $a_5 = 2.1239014(10^{-7})$

$a_1 = 6.3204790(10^0)$ $\quad$ $a_6 = -1.0067598(10^{-9})$

$a_2 = -1.4742752(10^{-1})$ $\quad$ $a_7 = 2.9480958(10^{-12})$

$a_3 = 2.5403593(10^{-3})$ $\quad$ $a_8 = -4.8430355(10^{-15})$

$a_4 = -2.8788220(10^{-5})$ $\quad$ $a_9 = 3.4075972(10^{-18})$

The latent heat (h_{fg}) was obtained by fitting the Keenan and Keyes' values on a power series. For P <400 psia,

$$h_{fg}(P) = \sum_{i=o}^{9} a_i P^i$$

$a_o = 9.9704457(10^2)$ $\quad$ $a_5 = -1.2499843(10^{-9})$

$a_1 = -2.1762821(10^0)$ $\quad$ $a_6 = 1.9322768(10^{-12})$

$a_2 = 1.9558791(10^{-2})$ $\quad$ $a_7 = -1.8023251(10^{-15})$

$a_3 = -1.2610018(10^{-4})$ $\quad$ $a_8 = 9.2680092(10^{-19})$

$a_4 = 5.0308804(10^{-7})$ $\quad$ $a_9 = -2.0148643(10^{-22})$

The values of the heat transfer area for the different tubes are:

TUBE		A (ft^2)
0.242 in. i.d. L/D =	30	0.038274
0.242	60	0.076548
0.242	90	0.114822
0.094	60	0.0154

The output data consisted of all the input variables and the computed quantities.

The program used for the L/D = 60, D = 0.094-in. test tube computation follows.

COMPUTATION PROGRAM

```
1  READ 2, I, J, K, PEXIT, E, CUR, HIN, W
   A       = .0154
   HADDED = 205.36 * E * CUR
   HTFLUX = HADDED / A
   BTULBM = HADDED / W
   P       = PEXIT
5 ENFPX = 1.1222734E2 + 6.3204790*P - 1.4742752E-1*(P**2)
 1 +2.5403593E-3 *(P**3) -2.8788220E-5*(P**4) +2.1239014E-7*(P**5)
 2 -1.0067598E-9*(P**6) +2.9480958E-12*(P**7)
 3 -4.8430355E-15*(P**8) +3.4075972E-18*(P**9)
6 ENFGPX=9.9704457E2 -2.1762821*P +1.9558791E-2*(P**2)
 1 -1.2610018E-4*(P**3) +5.0308804E-7*(P**4) -1.2499843E-9*(P**5)
 2 +1.9322768E-12*(P**6) -1.8023251E-15*(P**7)
 3 +9.2680092E-19*(P**8) -2.0148643E-22*(P**9)
   X = (HIN + BTULBM - ENFPX)/ENFGPX
   PRINT 3, I, J, K, PEXIT, E,
 1  CUR, HIN, W, HADDED, HTFLUX, BTULBM, X, ENFPX, ENFGPX
   GO TO 1
2  FORMAT (315,5E10.2)
3  FORMAT (7HORUN NOI3, 1H-, I3, 1H-,13,5X,
 1 6HPEXIT=E15.6,5X,2HE=E15.6,5X,4HCUR=E15.6/5X,
 2 4HHIN=E15.6,5X2HW=E15.6,5X,7
 3 HHADDED=E15.6/5X,7HHTFLUX=E15.6,5X,
 4 7HBTULBM=E15.6,5X,2HX=E15.6/5X
 5 6HENFPX=E15.6,5X,7HENFGPX=E15.6)
  END
```

APPENDIX D

Incipient Boiling Analysis

The effects of velocity, temperature, and pressure on the incipient boiling heat flux, $(q/A)_i$, can be examined by means of the correlations given in Ref. 22. This correlation for water is:

$$(q/A)_i = 15.60\ P^{1.156}(T_w-T_s)^{\frac{2.30}{P^{.0234}}} \qquad (D1)$$

For a uniformly heated tube the heat flux can be calculated from:

$$(q/A) = h(T_w-T_b) = h\ (T_w-T_s) + (T_s-T_b) \qquad (D2)$$

The saturation temperature is known from the exit pressure. The bulk temperature is found by the First Law:

$$q = c_p(T_{out}-T_{in})w \qquad (D3)$$

which leads to:

$$T_{out} = (q/A)\frac{A}{wc_p} + T_{in} = T_b\ . \qquad (D4)$$

Since the probe is at the exit, only the conditions at the exit are of interest and therefore $T_b = T_{out}$. The heat transfer coefficient, h, is found using McAdams' correlation:[26]

$$(\frac{hD}{k}) = 0.023\ (\frac{GD}{\mu})^{.8}(\frac{\mu c_p}{k})^{.4} \qquad (D5)$$

where the properties are evaluated at the bulk fluid temperature. For the actual numerical analysis, the values of these properties came from ElWakil.[27] By assuming a value of

(q/A), T_b and hence h can be calculated. Then using (D2), (T_w-T_s) is found. The values of (q/A) and (T_w-T_s), for various, G, T_i, and P_e can then be found and plotted. Equation (D1) for the various pressures is then superimposed on these plots. The intersections of the (q/A) vs. (T_w-T_s) curve and the $(q/A)_i$ curve is the point at which incipient boiling is predicted.

This analysis was carried out for the conditions that were presented in Figs. 28 through 31, i.e.

	$G \times 10^{-6}$ lbm/hr-ft^2	T_i °F	P_e (psia)
a)	0.4	100, 150, 200	30
b)	0.4	100, 200	100
c)	2.0	100, 150, 200	30
d)	2.0	100, 200	100

In Fig. 32a is a representative plot for the conditions in (c). To visually relate the predicted $(q/A)_i$ to (x), operating lines obtained from the formula:

$$x = \frac{q/w + h_{in} - h_f}{h_{fg}} \qquad (D6)$$

are plotted on coordinates of (q/A) vs x. The $(q/A)_i$ found from the analysis are plotted on these operating lines and are connected by a smooth line. This line then is the locus of predicted $(q/A)_i$ for various inlet temperatures. This plot for conditions (c) above is presented in Fig. 32b. Examining Fig. 32b it is seen that incipient boiling occurs at greater subcoolings for lower T_i. From the analysis of

conditions a, b, d, it was also found that incipient boiling occurs at greater subcooling for larger pressures and, keeping P and T_i constant, at higher G.

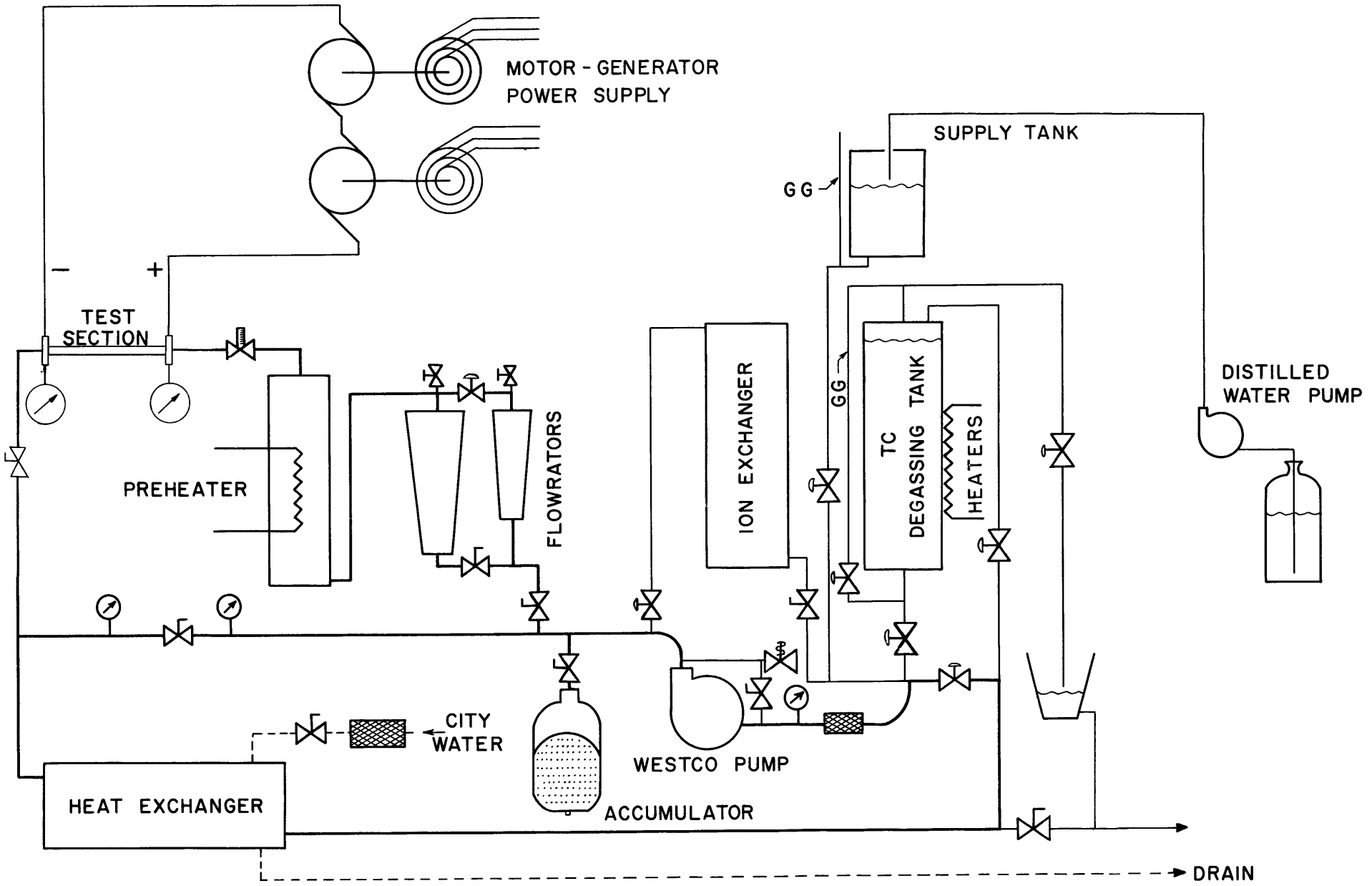

FIG. 1 SCHEMATIC LAYOUT OF TEST FACILITY

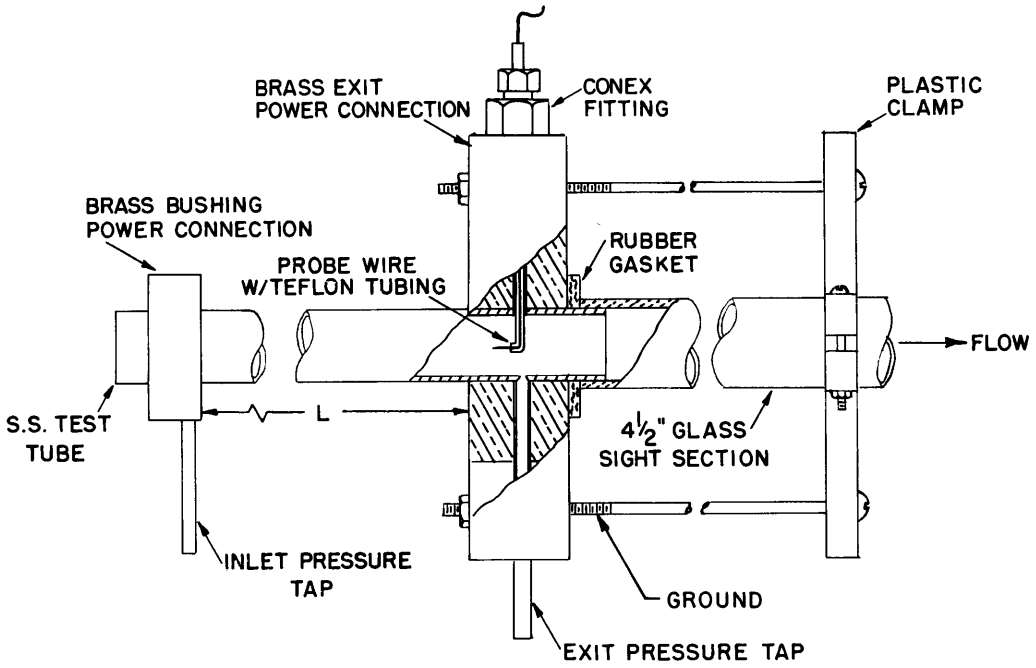

RESISTANCE PROBE AND TEST SECTION

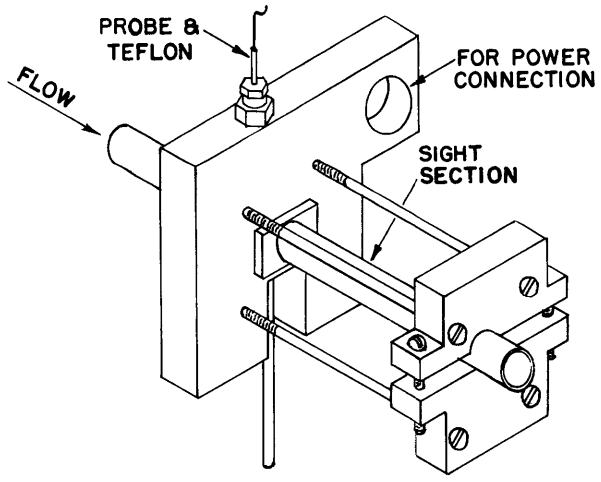

TEST SECTION EXIT
WITH SIGHT SECTION

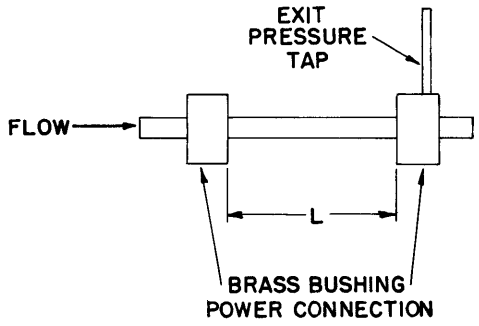

BURNOUT TEST SECTION

FIG. 2 DETAILED VIEW OF TEST SECTIONS

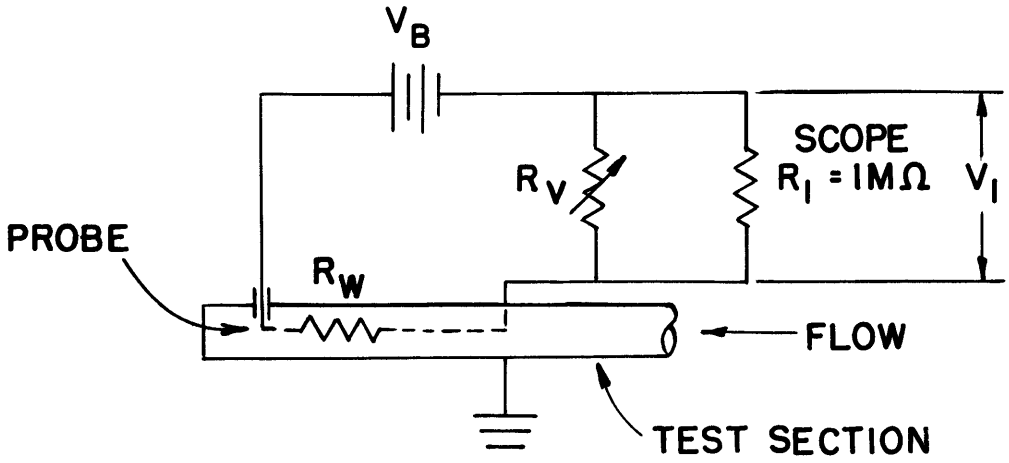

FIG. 3a PROBE CIRCUIT DIAGRAM

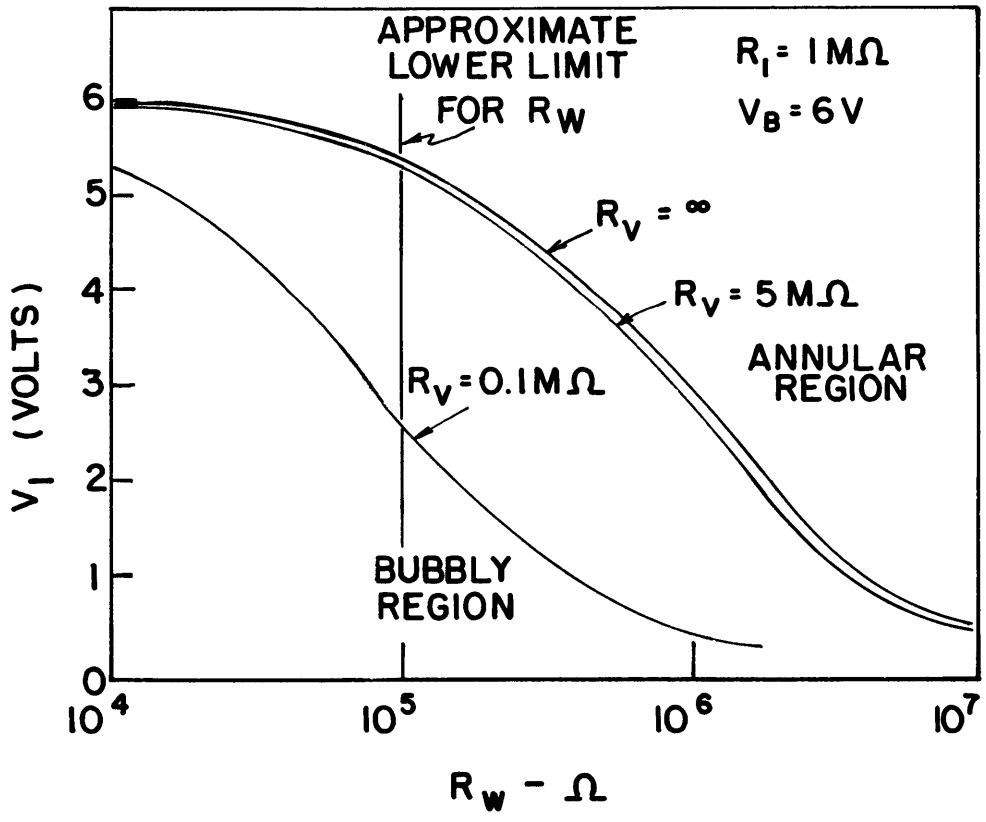

FIG. 3b CHARACTERISTICS OF PROBE CIRCUIT

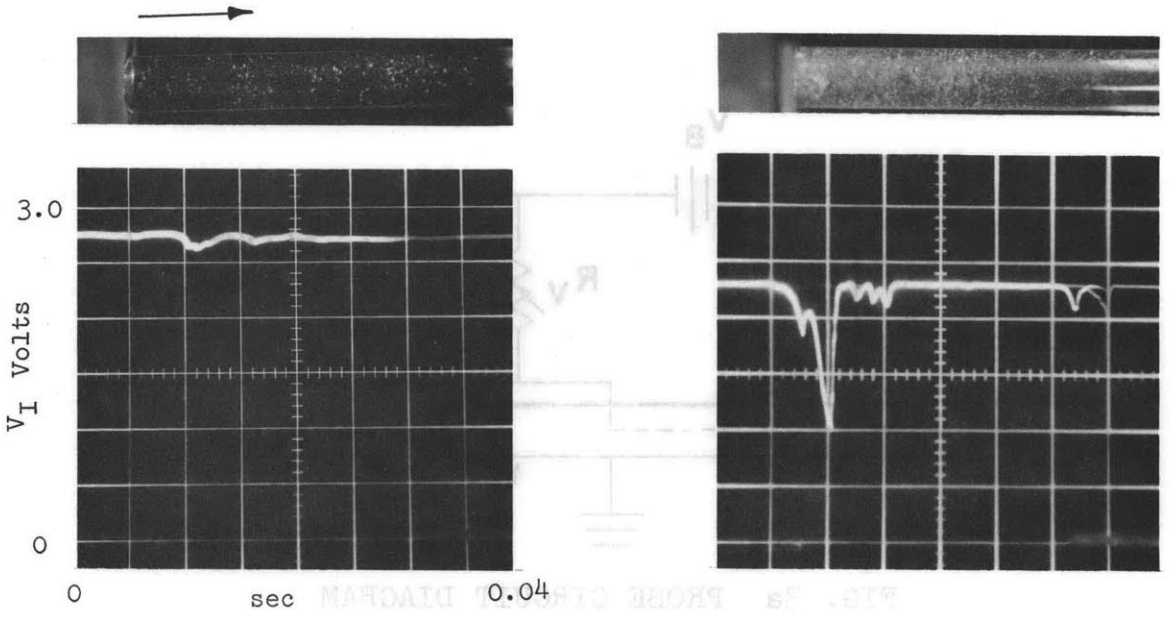

PHOTO I

P~30, G=0.8x10^6, T_i=200, x=-0.67%

BUBBLY

PHOTO II

P~30, G=2.0x10^6, T_i=200, x=-2.81%

BTS TRANSITION

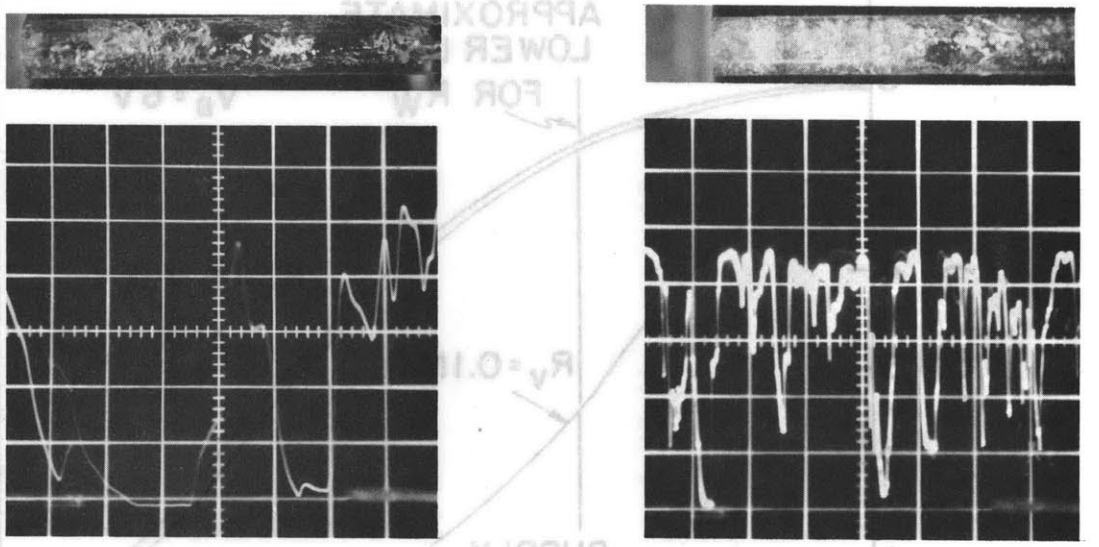

PHOTO III

P~30, G=0.4x10^6, T_i=150, x=-.201%

SLUG

PHOTO IV

P~30, G=2.0x10^6, T_i=100, x=-1.43%

SLUG

FIG. 4 COMPARISON OF PROBE AND SIGHT-SECTION OBSERVATIONS (BUBBLY, BUBBLY-TO-SLUG, SLUG)

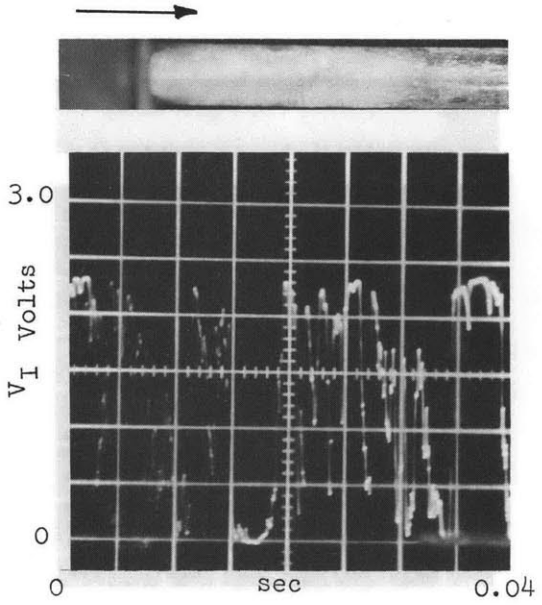

PHOTO V

P~30, G=2.0x10^6, T_i=100, x=0.25%

FIRST INDICATION OF STA TRANSITION

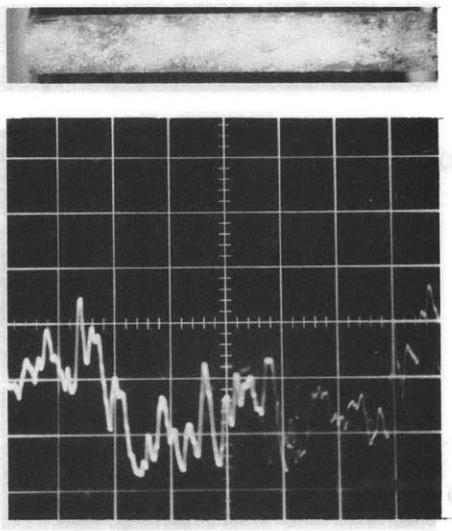

PHOTO VI

P~30, G=0.8x10^6, T_i=100, x=2.42%

STA TRANSITION

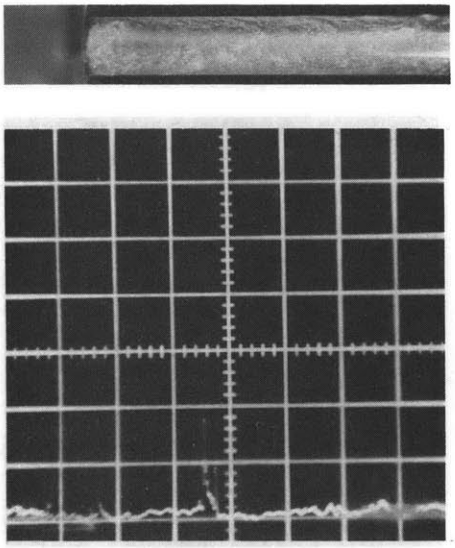

PHOTO VII

P~30, G=0.4x10^6, T_i=200, x=10.99%

ANNULAR

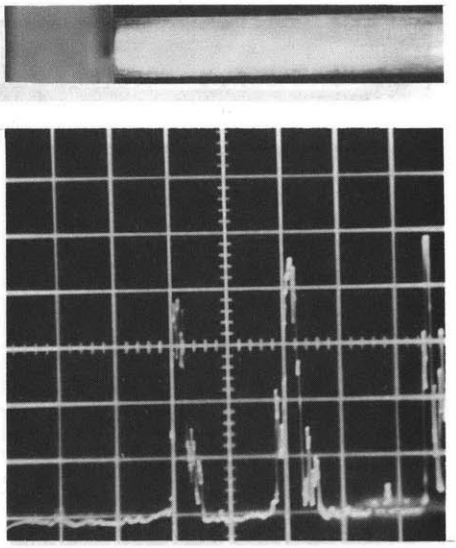

PHOTO VIII

P~30, G=1.2x10^6, T_i=100, x=7.7%

ANNULAR

FIG. 5 COMPARISON OF PROBE AND SIGHT-SECTION OBSERVATIONS (SLUG-TO-ANNULAR, ANNULAR)

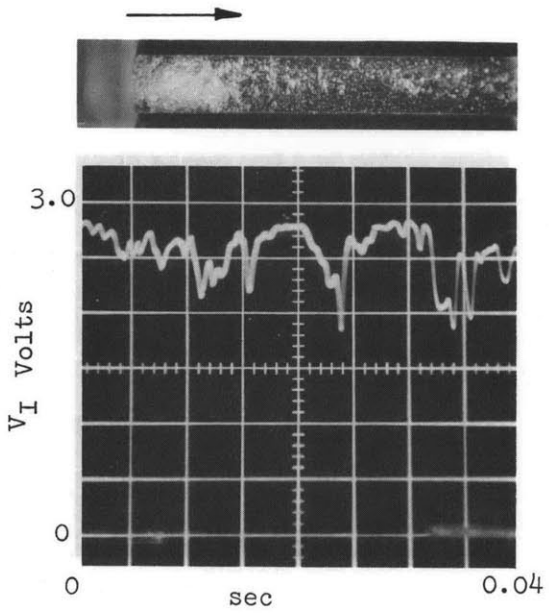

PHOTO IX

P~30, G=2.0x10^6, T_i=200, x=-0.78%

WISPY ANNULAR

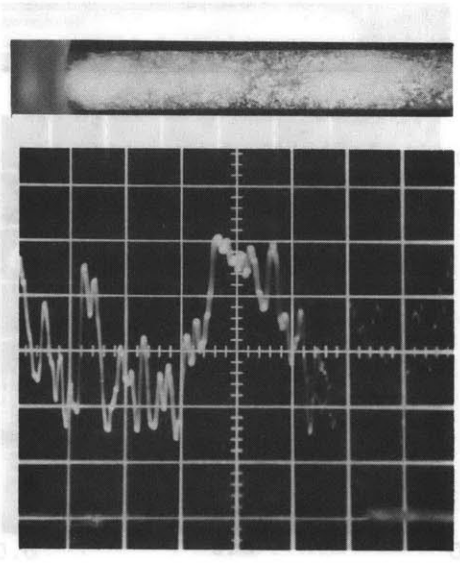

PHOTO X

P~30, G=2.0x10^6, T_i=200, x=-0.68%

WISPY ANNULAR

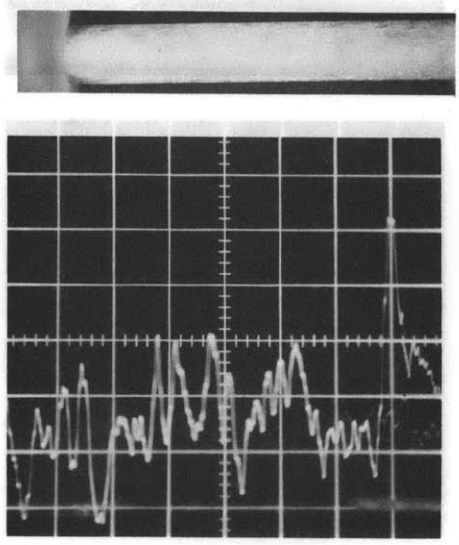

PHOTO XI

P~30, G=2.0x10^6, T_i=200, x=4.69%

WISPY ANNULAR

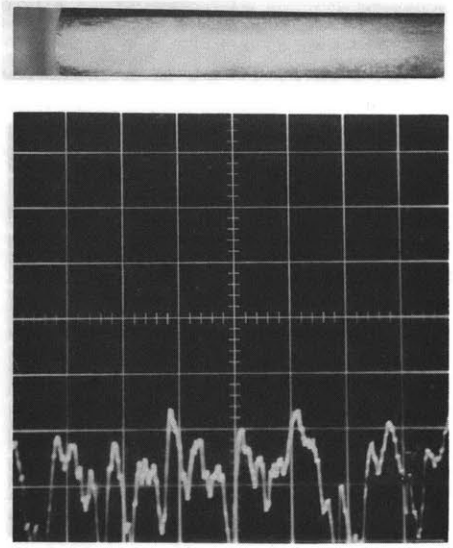

PHOTO XII

P~30, G=0.8x10^6, T_i=200, x=11.05%

ANNULAR WITH NEGATIVE CHARGE EFFECT

FIG. 6 COMPARISON OF PROBE AND SIGHT-SECTION OBSERVATIONS (WISPY ANNULAR)

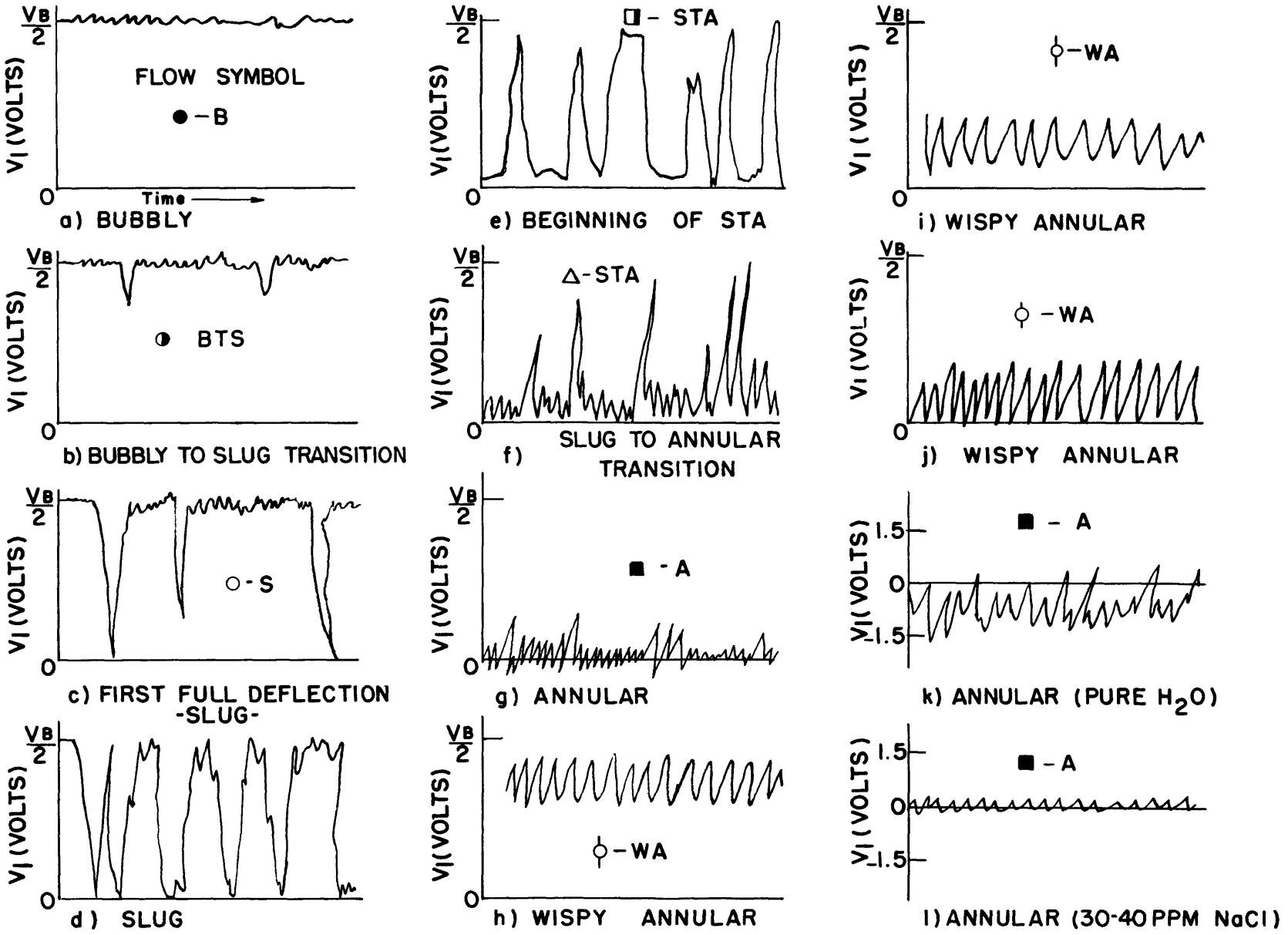

FIG. 7 SCHEMATIC OF VOLTAGE TRACES FOR VARIOUS FLOW REGIMES

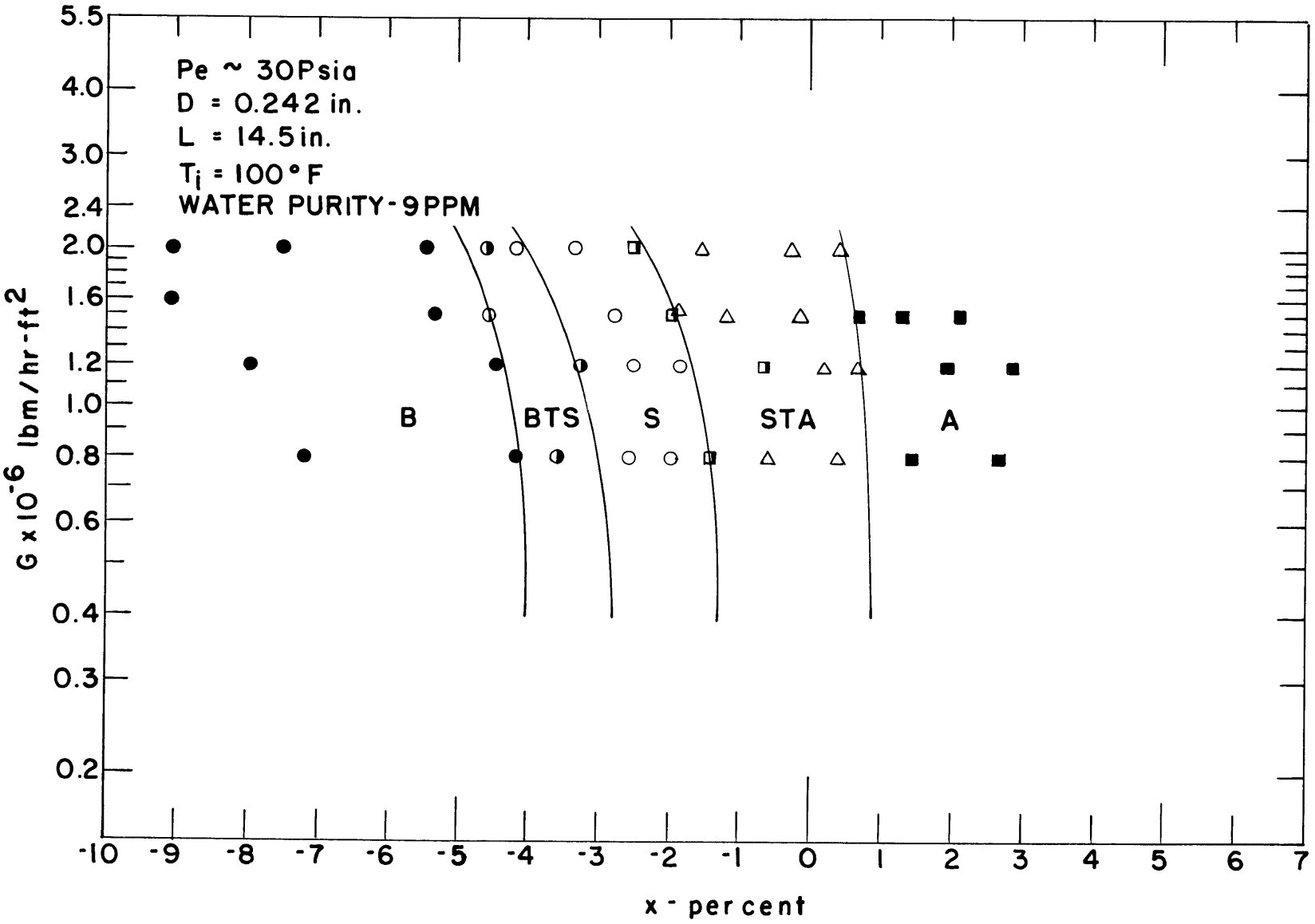

FIG. 8 FLOW REGIME MAP - WATER PURITY = 9PPM NaCl

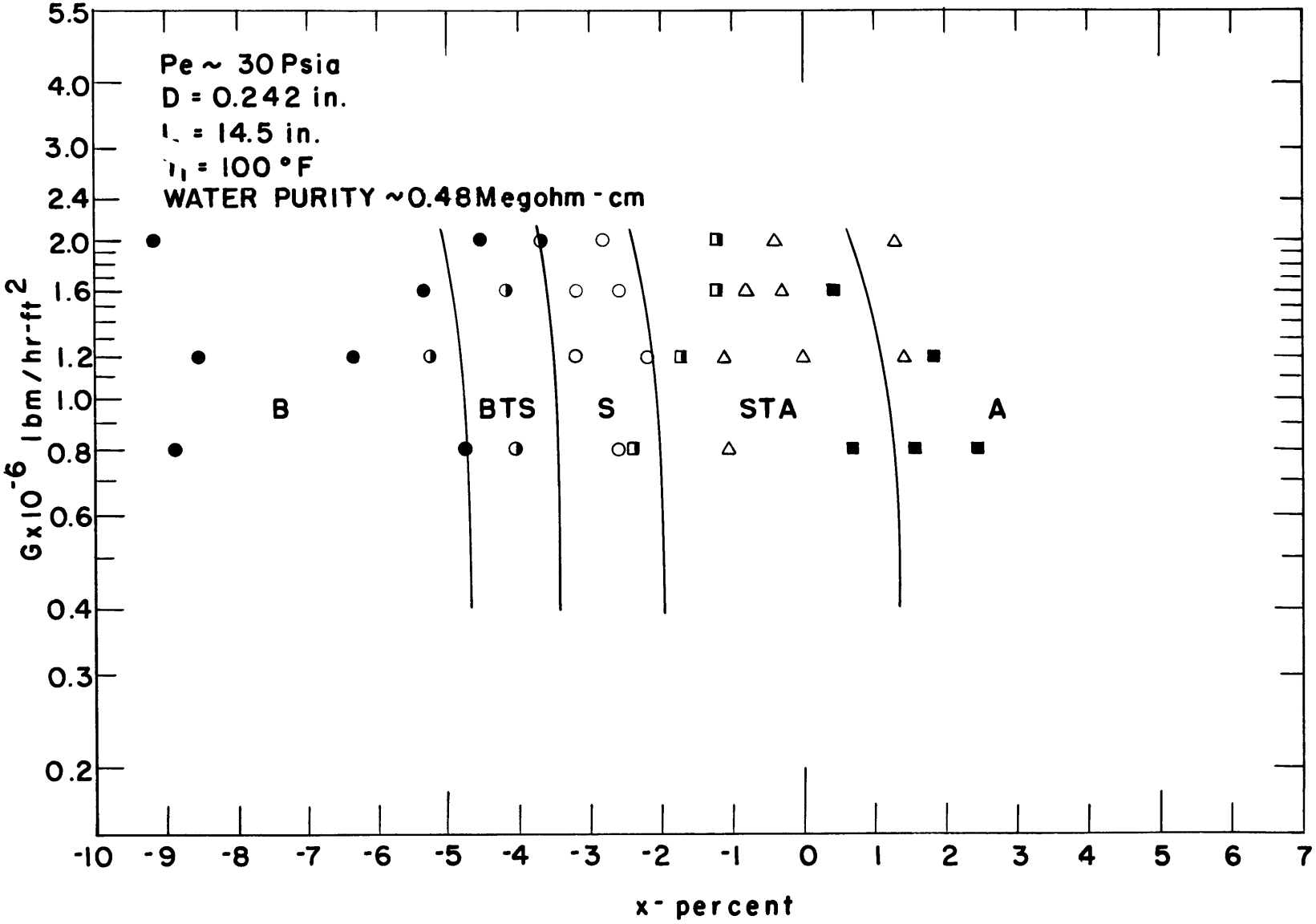

FIG. 9 FLOW REGIME MAP - WATER PURITY = 0.48 Megohm-cm

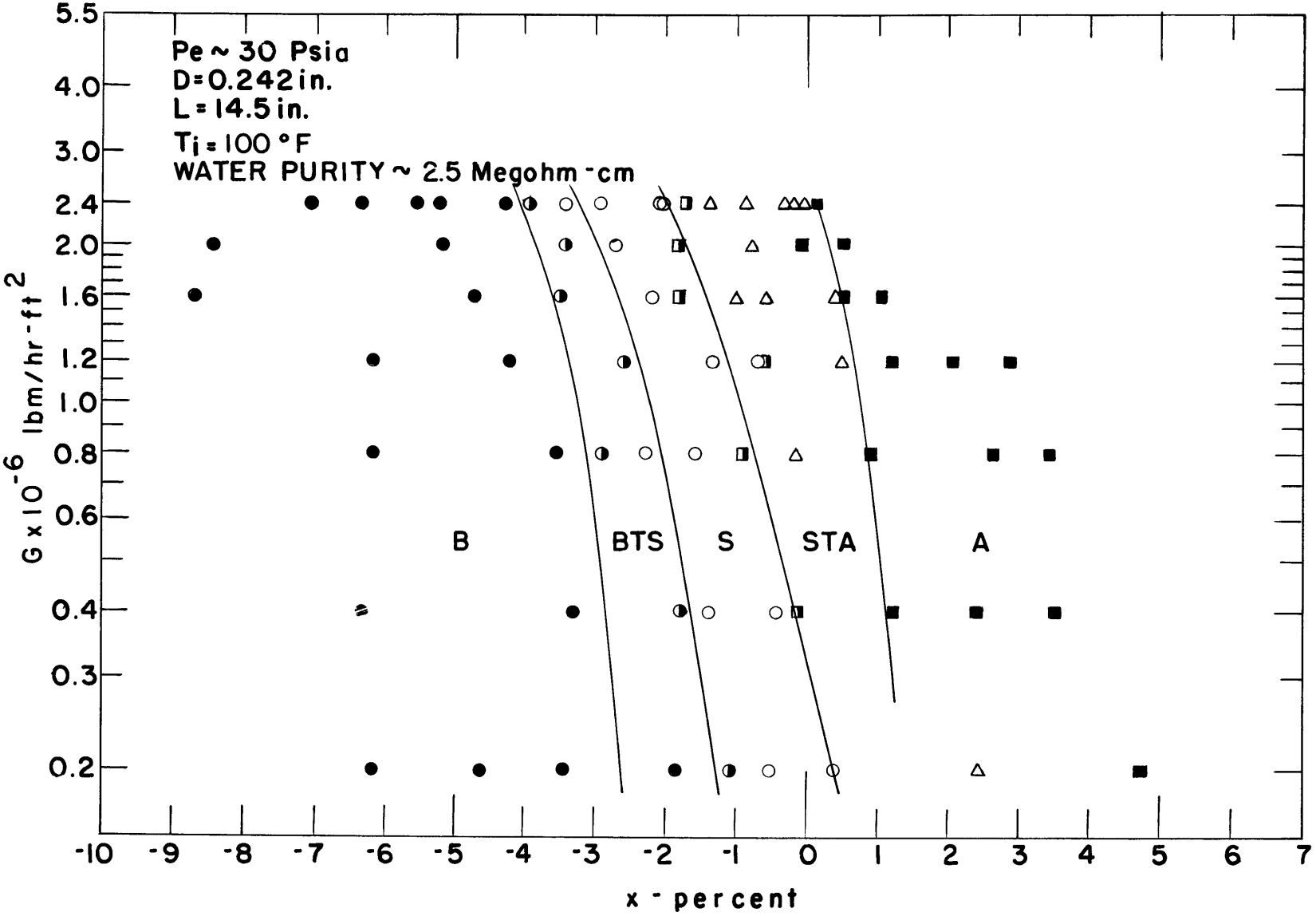

FIG. 10 FLOW REGIME MAP - WATER PURITY = 2.5 Megohm-cm

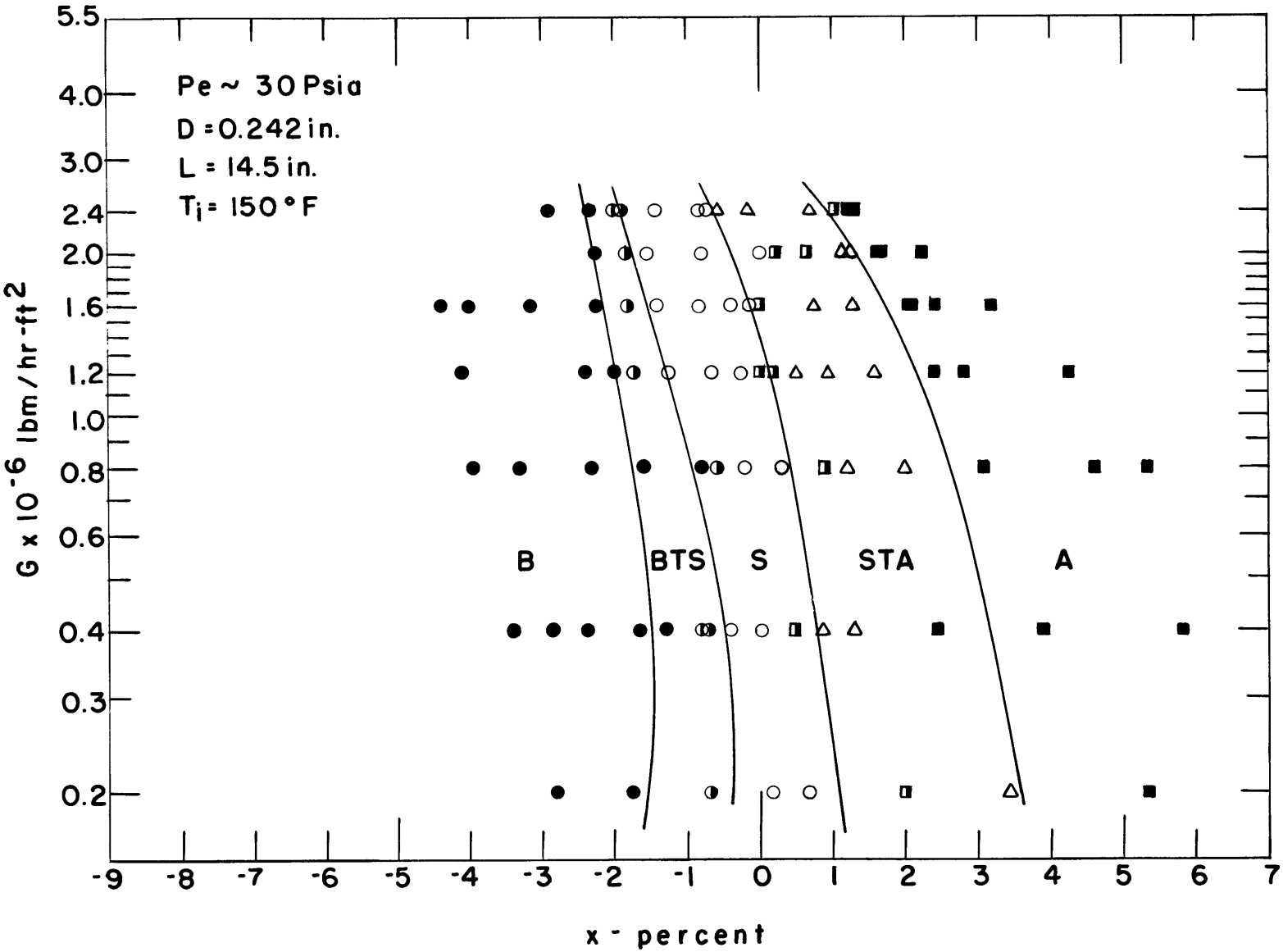

FIG. 11 FLOW REGIME MAP - T_i = 150°F, LOW PRESSURE

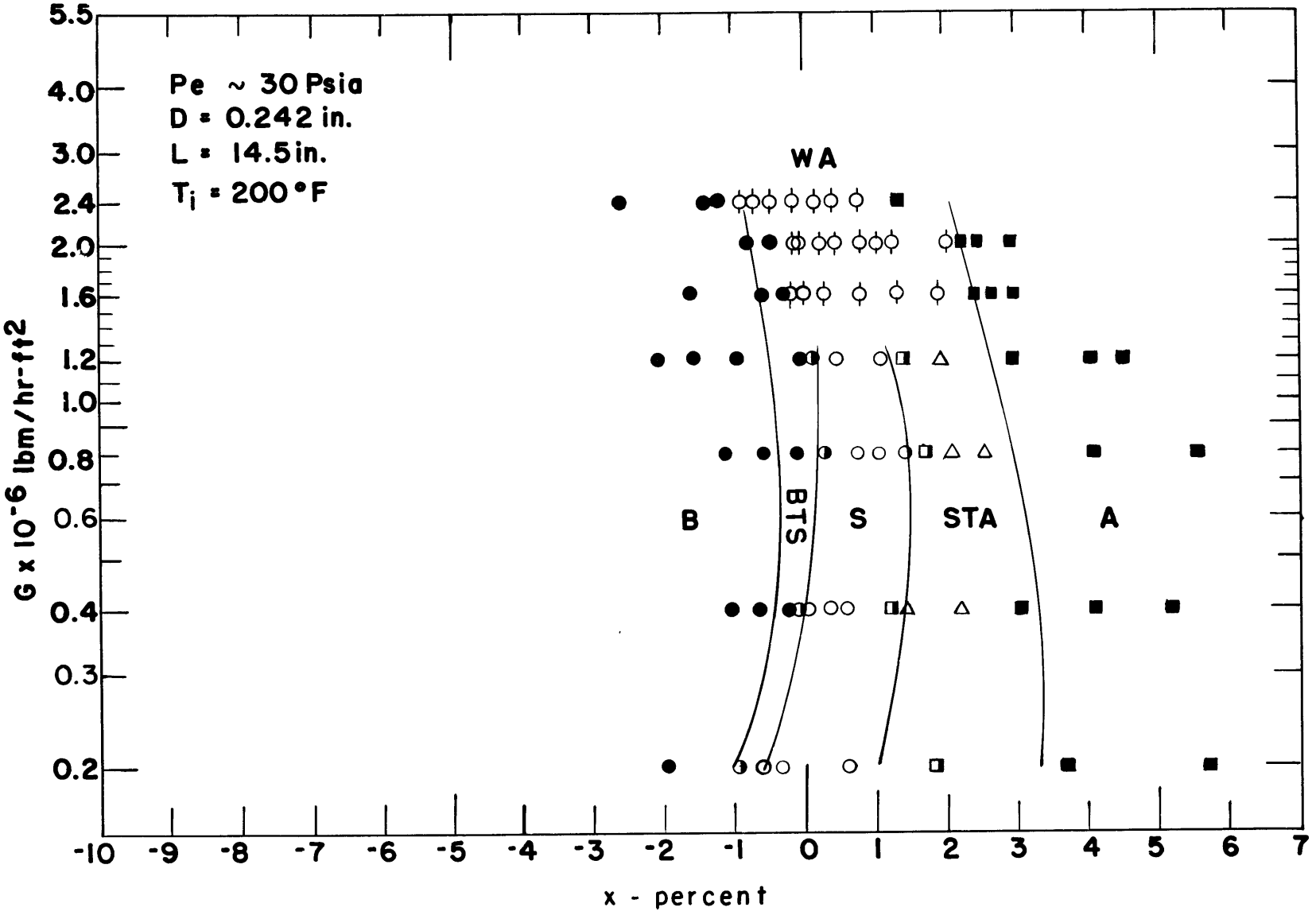

FIG. 12 FLOW REGIME MAP - T_i = 200°F, LOW PRESSURE

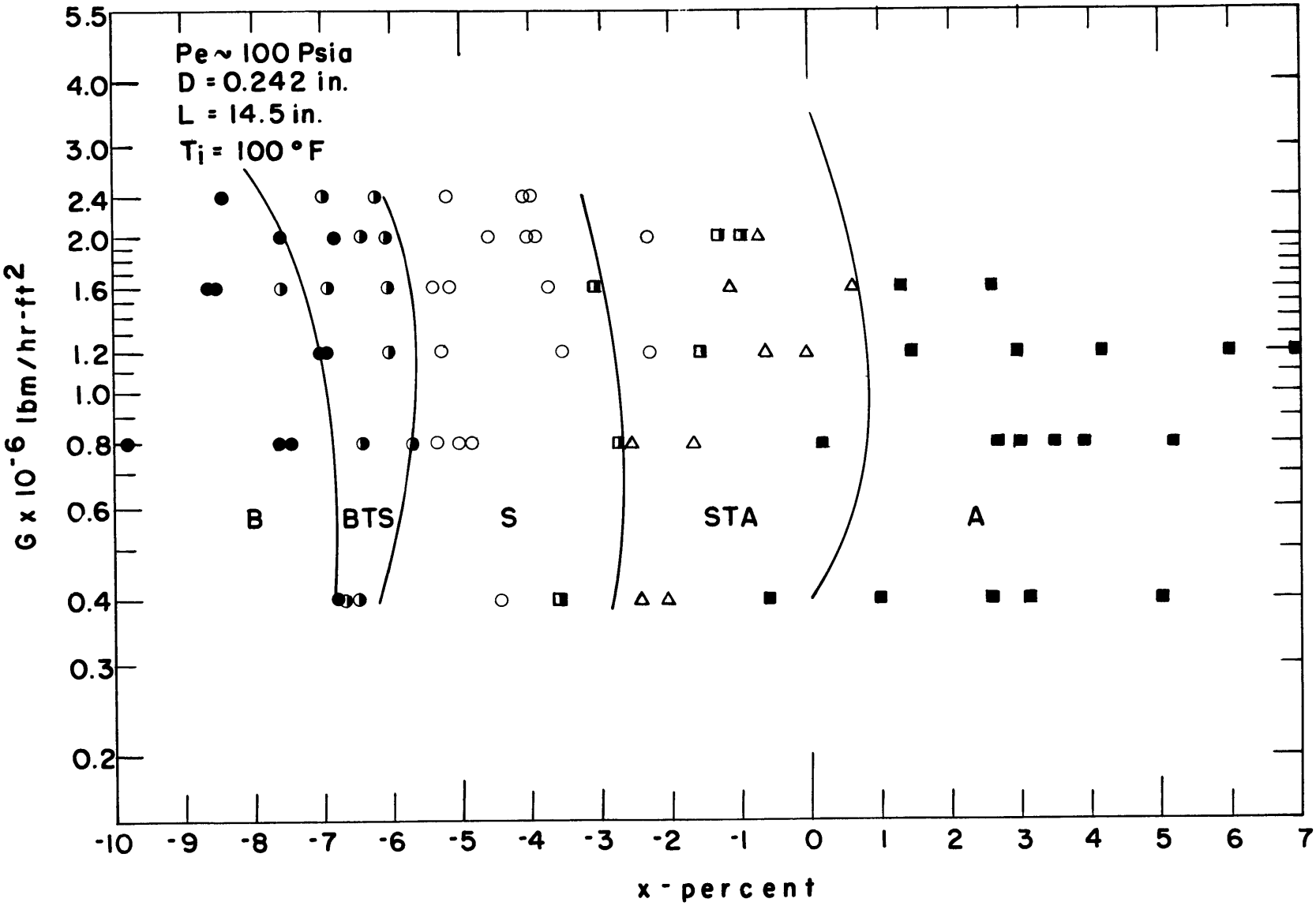

FIG. 13 FLOW REGIME MAP - HIGH PRESSURE, T_i = 100°F

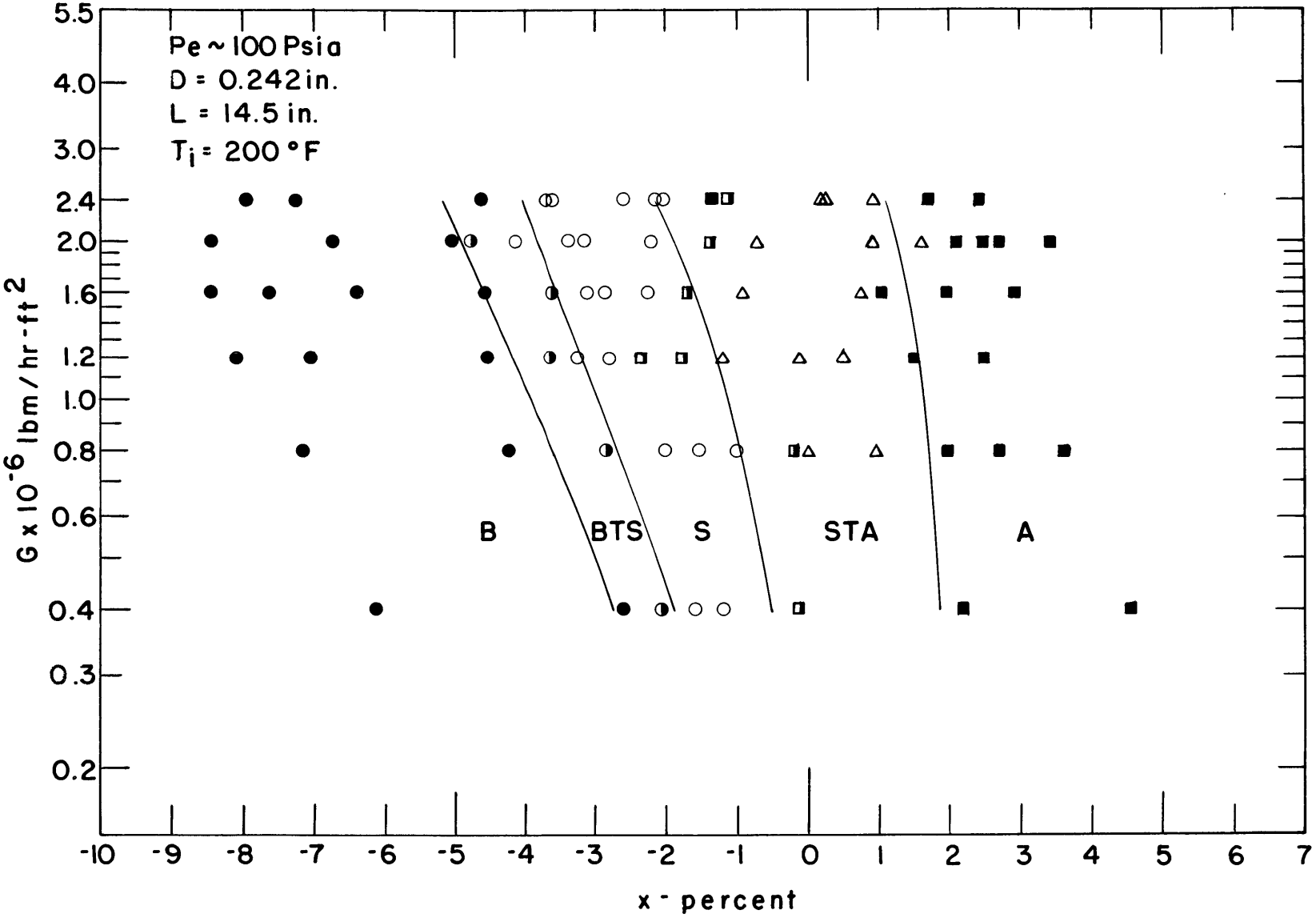

FIG. 14 FLOW REGIME MAP - HIGH PRESSURE, T_i = 200°F

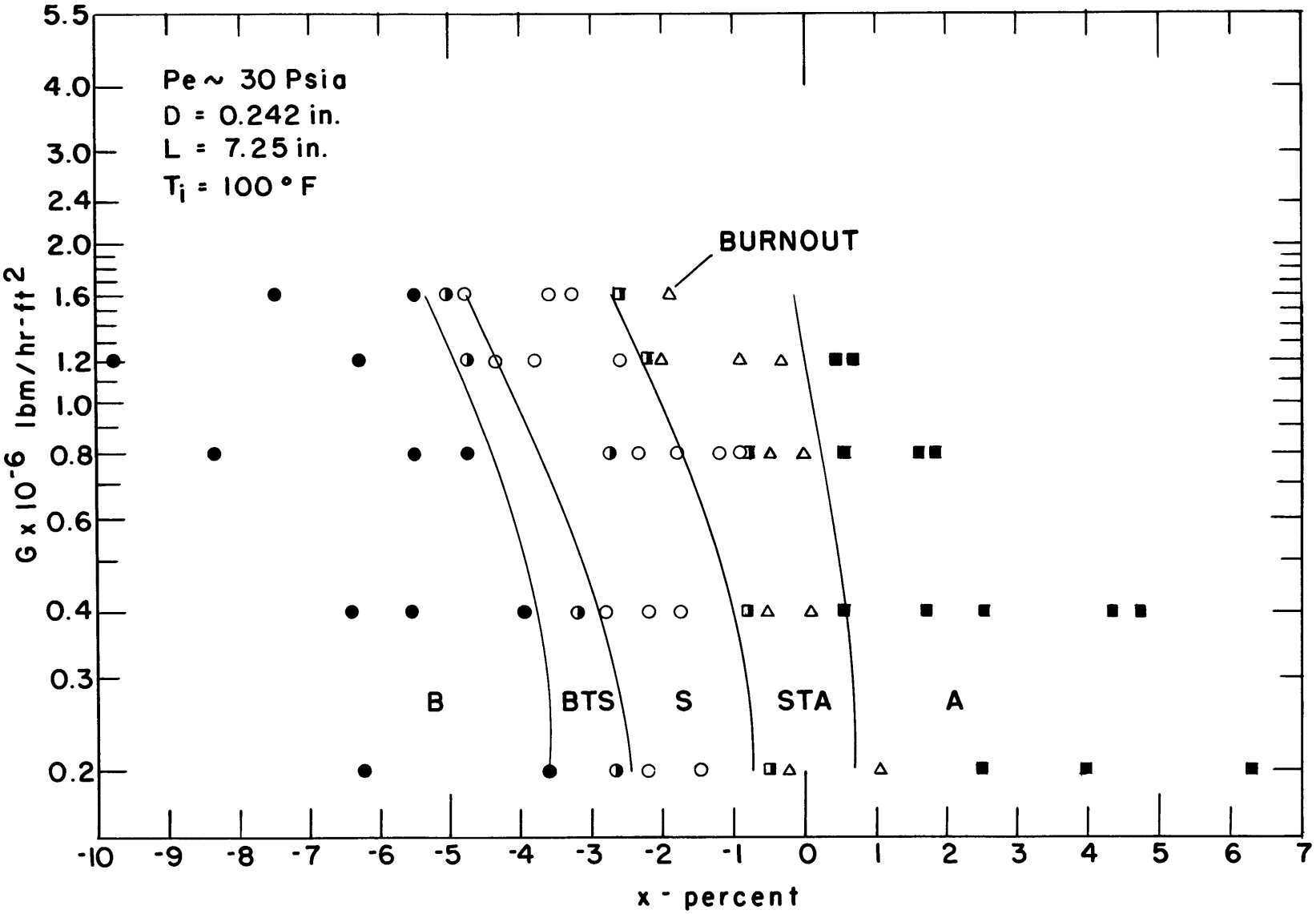

FIG. 15 FLOW REGIME MAP - L/D = 30

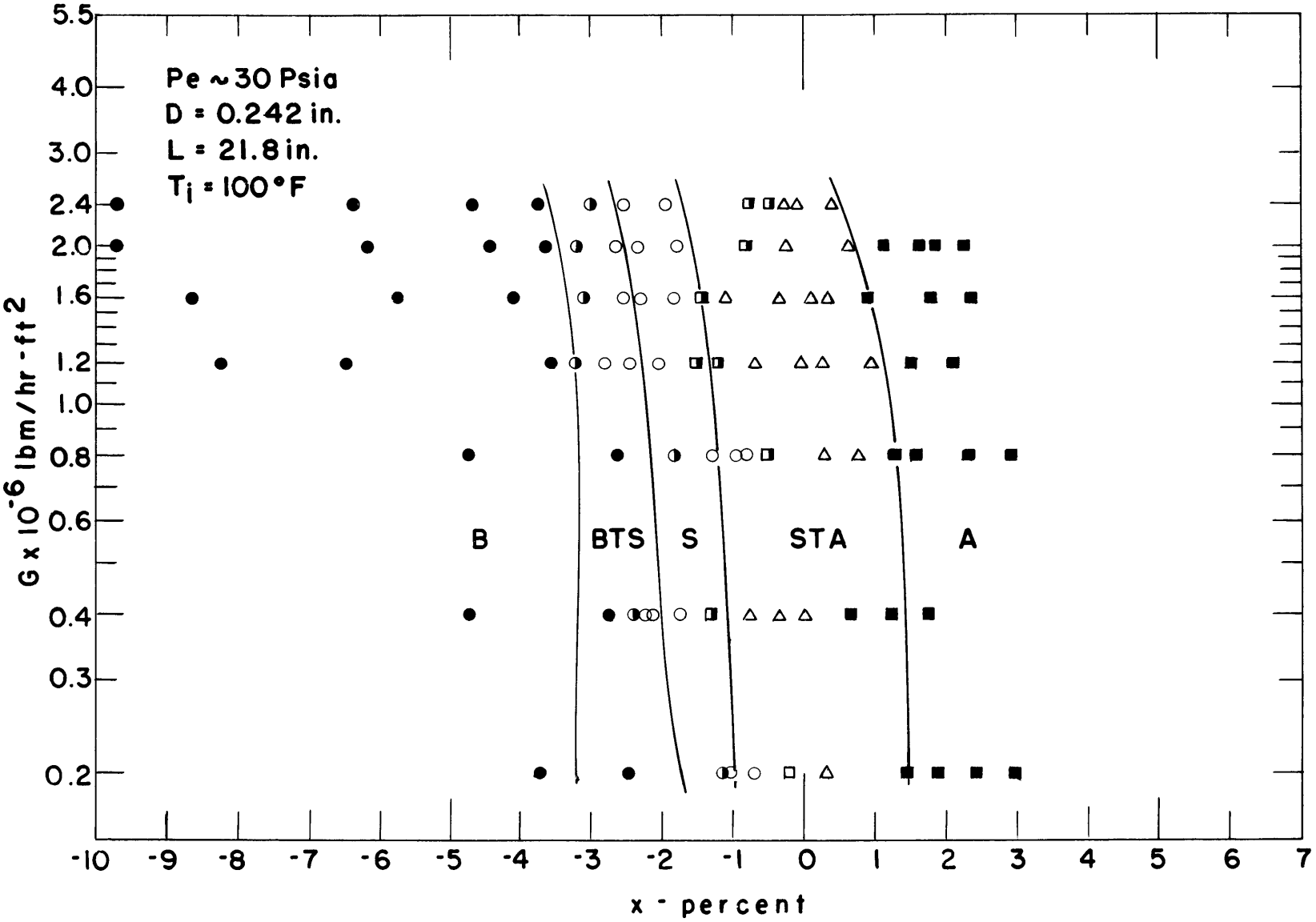

FIG. 16 FLOW REGIME MAP - L/D = 90

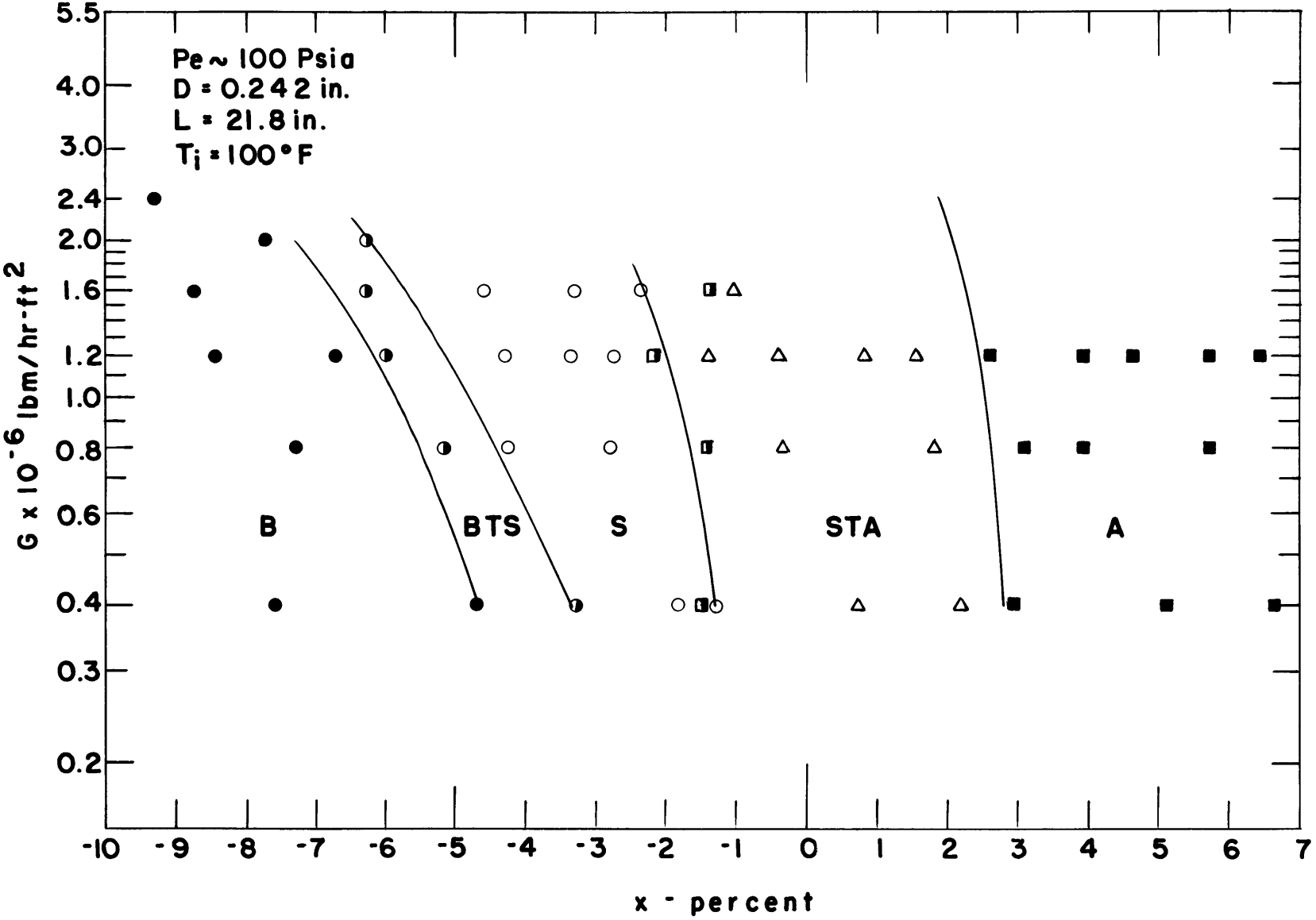

FIG. 17 FLOW REGIME MAP - L/D = 90, HIGH PRESSURE

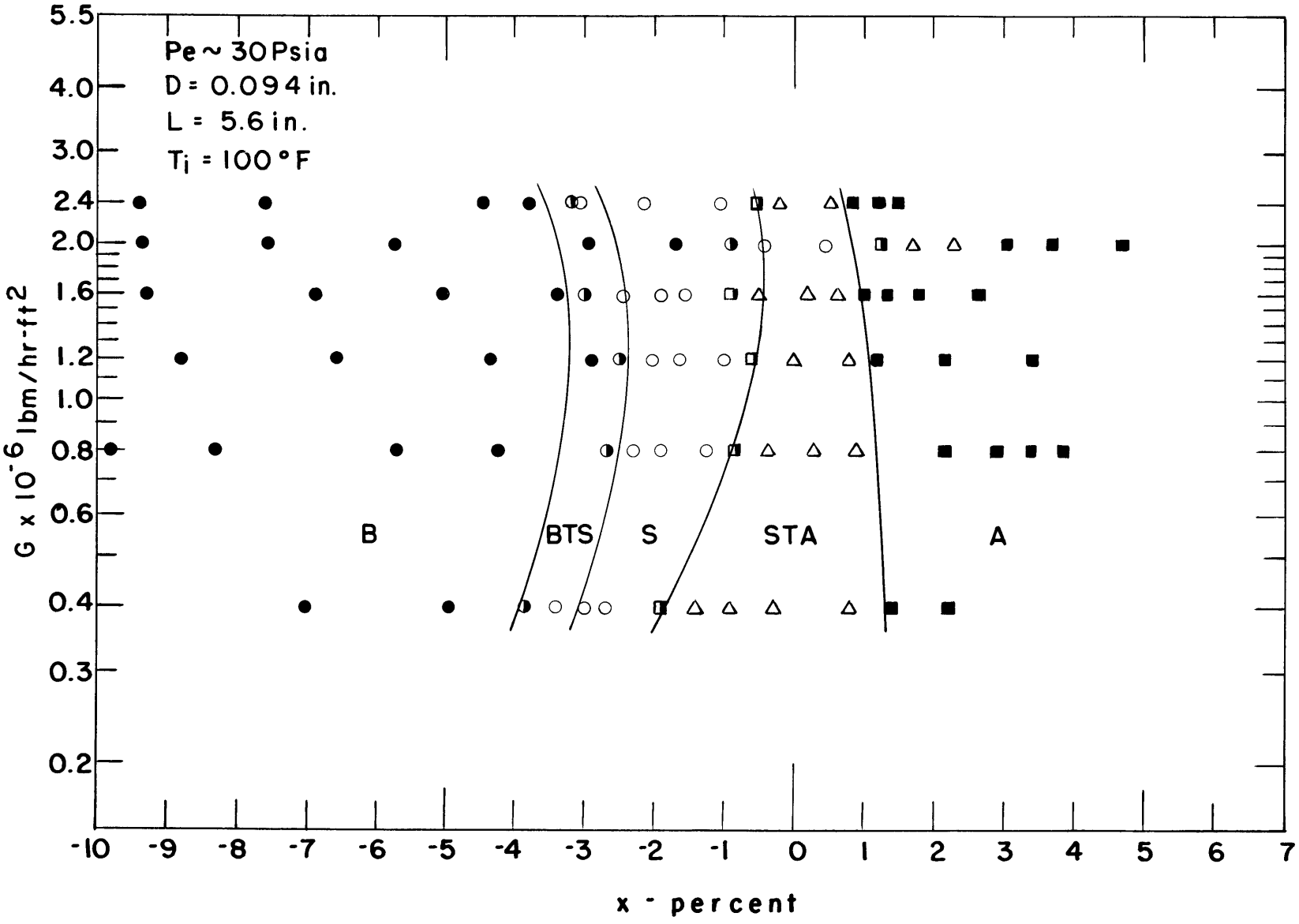

FIG. 18 FLOW REGIME MAP - D = 0.094 in., T_i = 100°F

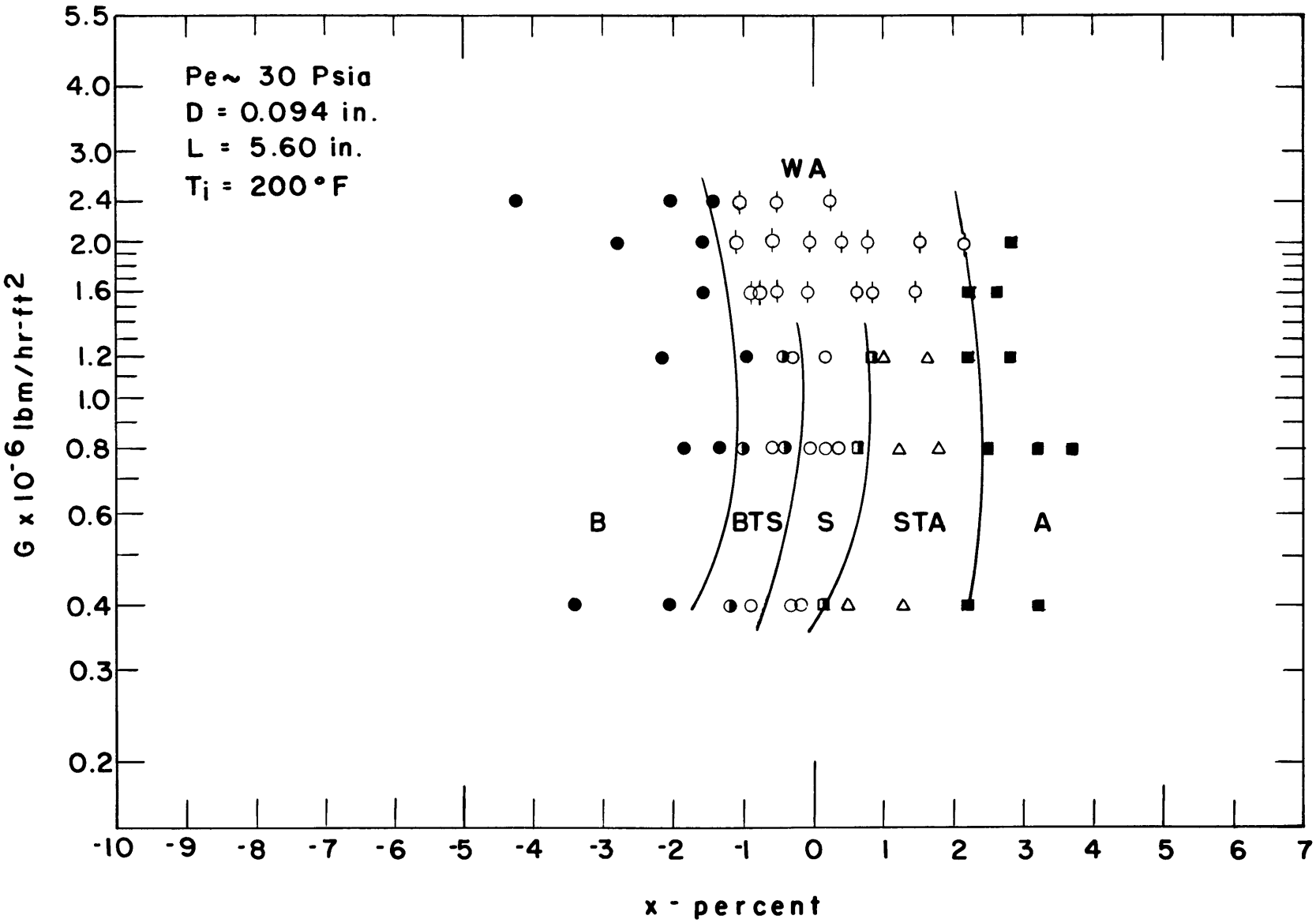

FIG. 19 FLOW REGIME MAP - D = 0.094 in., T_i = 200°F

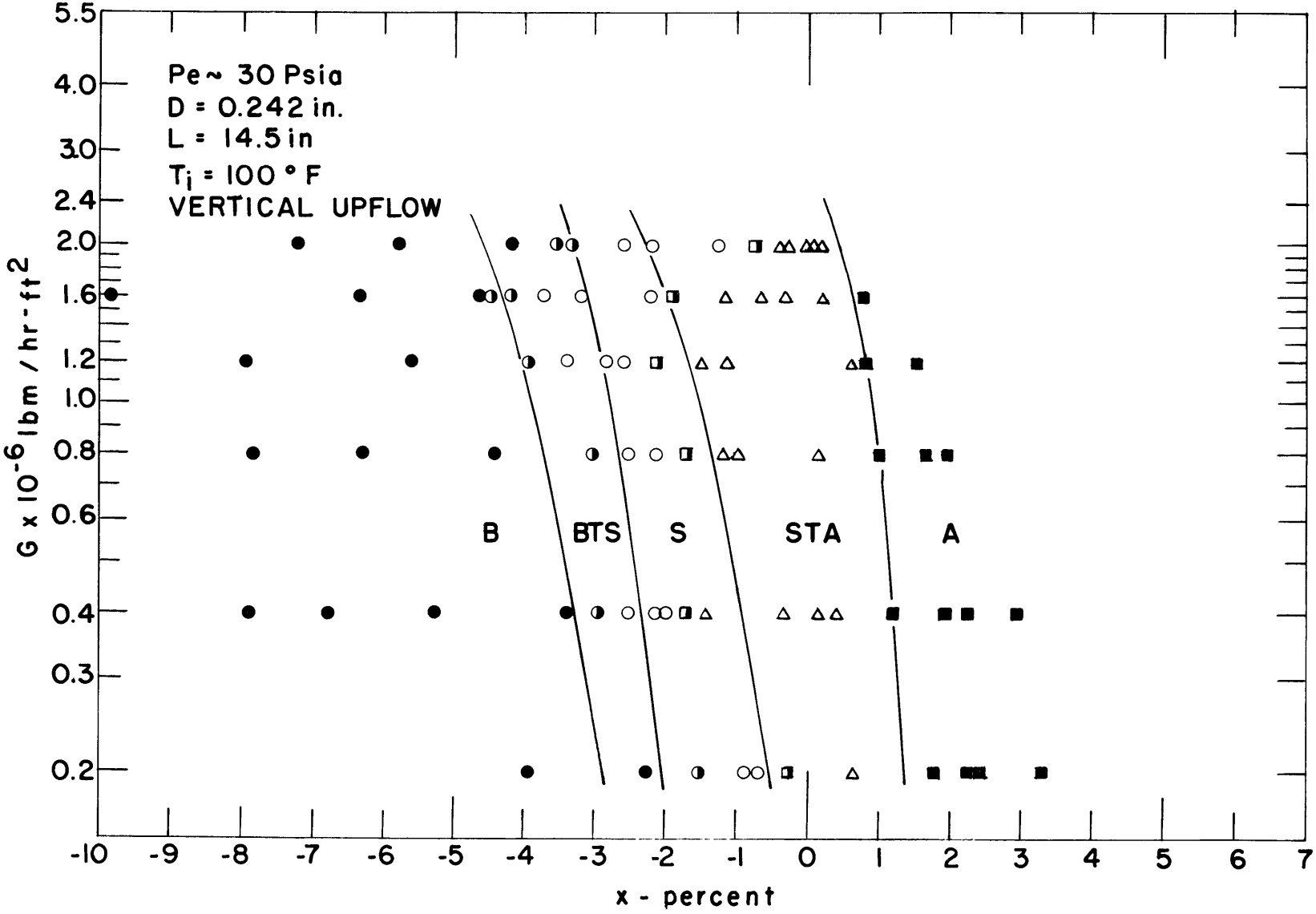

FIG. 20 FLOW REGIME MAP - VERTICAL UPFLOW

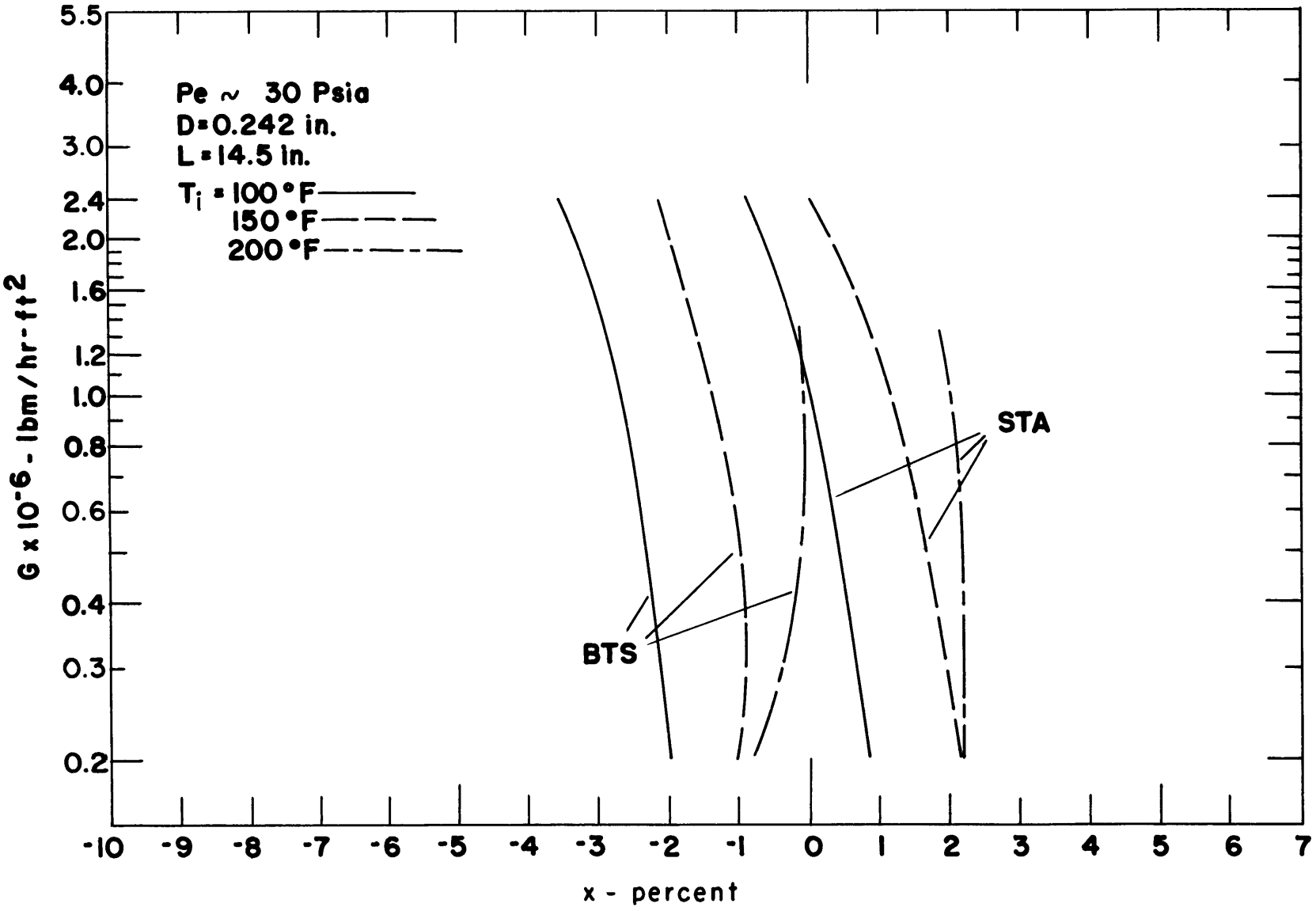

FIG. 21 EFFECT OF INLET TEMPERATURE ON FLOW REGIME BOUNDARIES - $P_e \sim 30$ psia

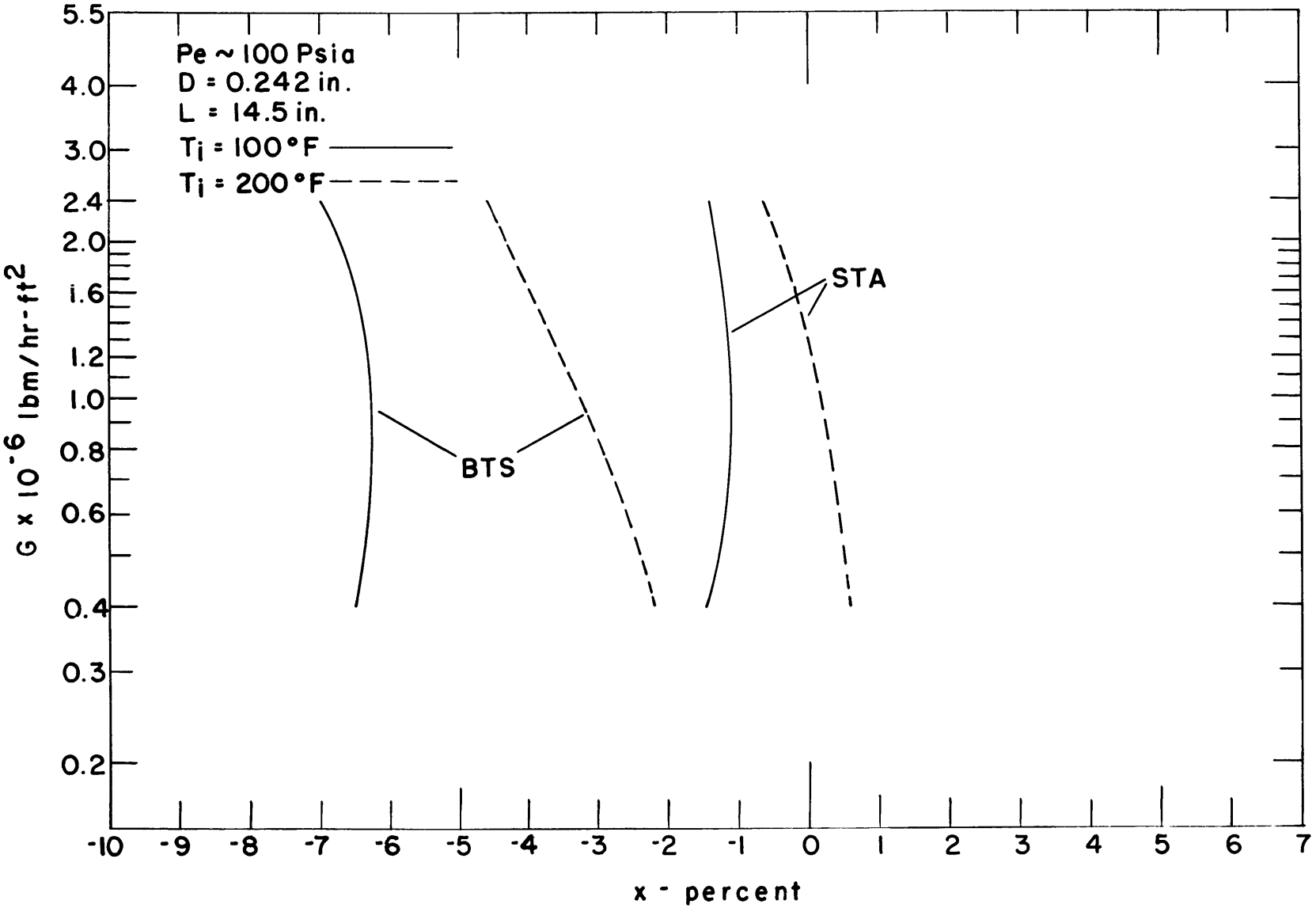

FIG. 22 EFFECT OF INLET TEMPERATURE ON FLOW REGIME BOUNDARIES - $P_e \sim$ 100 psia

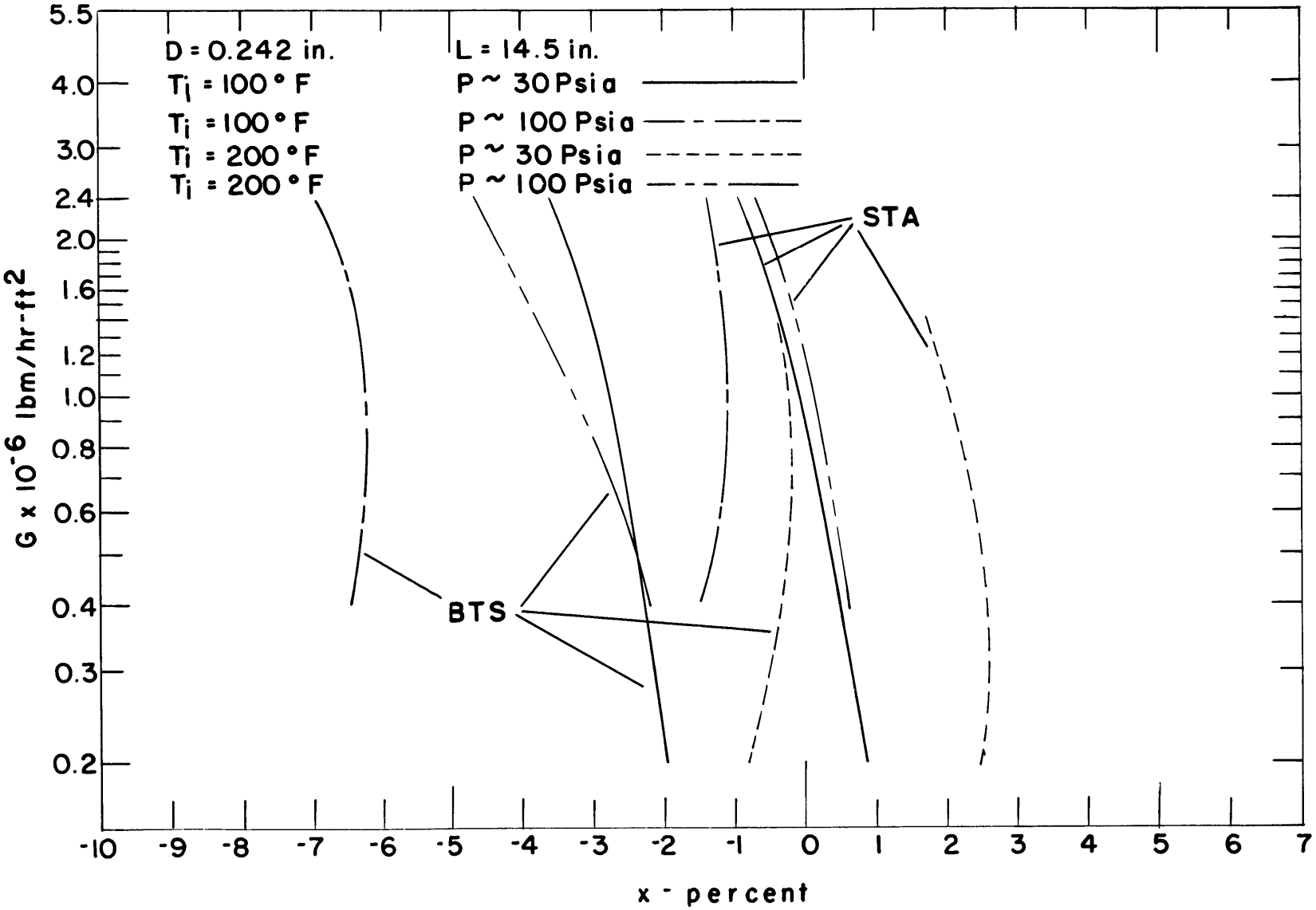

FIG. 23 EFFECT OF EXIT PRESSURE ON FLOW REGIME BOUNDARIES

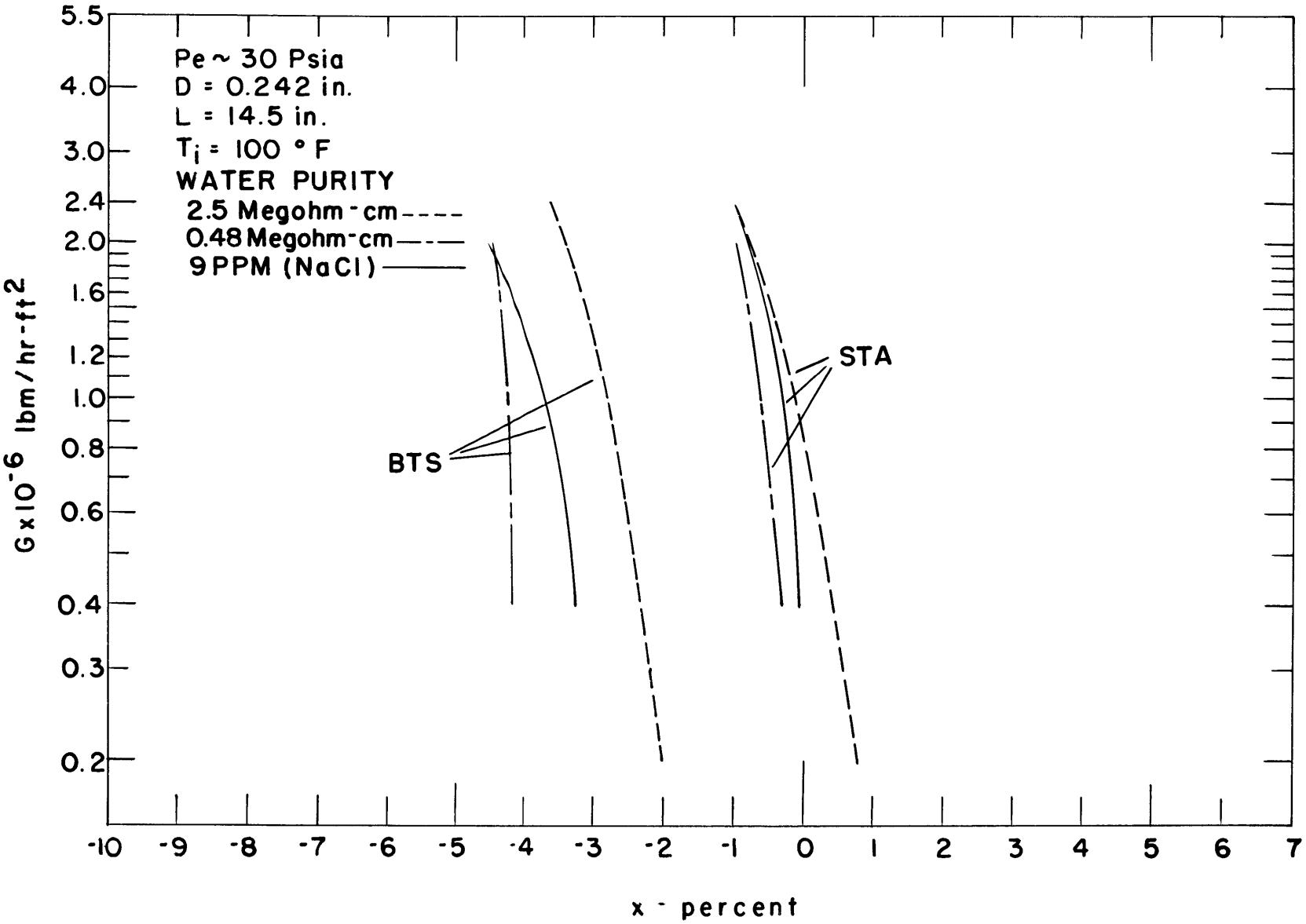

FIG. 24 EFFECT OF WATER PURITY ON FLOW REGIME BOUNDARIES

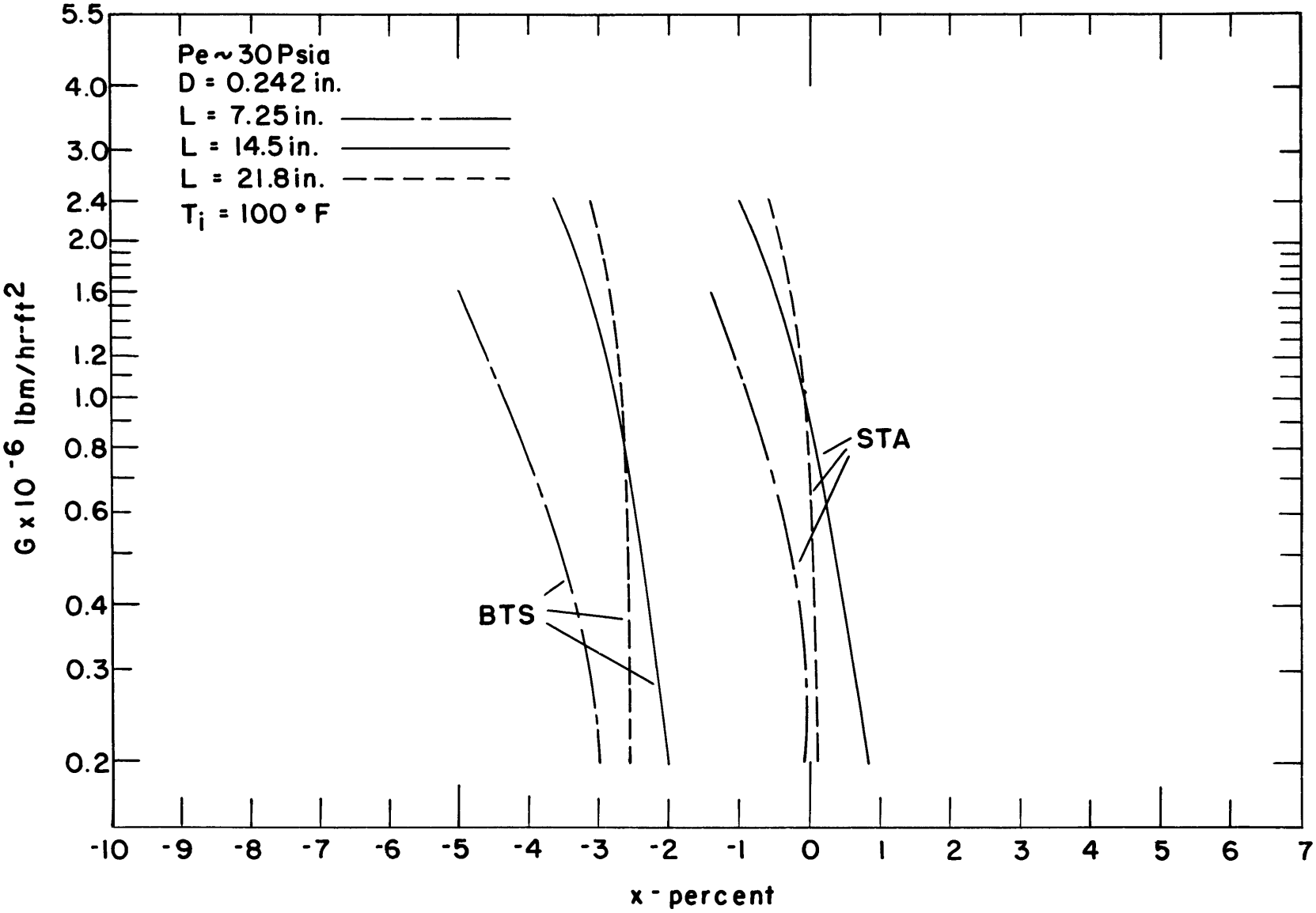

FIG. 25 EFFECT OF LENGTH ON FLOW REGIME BOUNDARIES

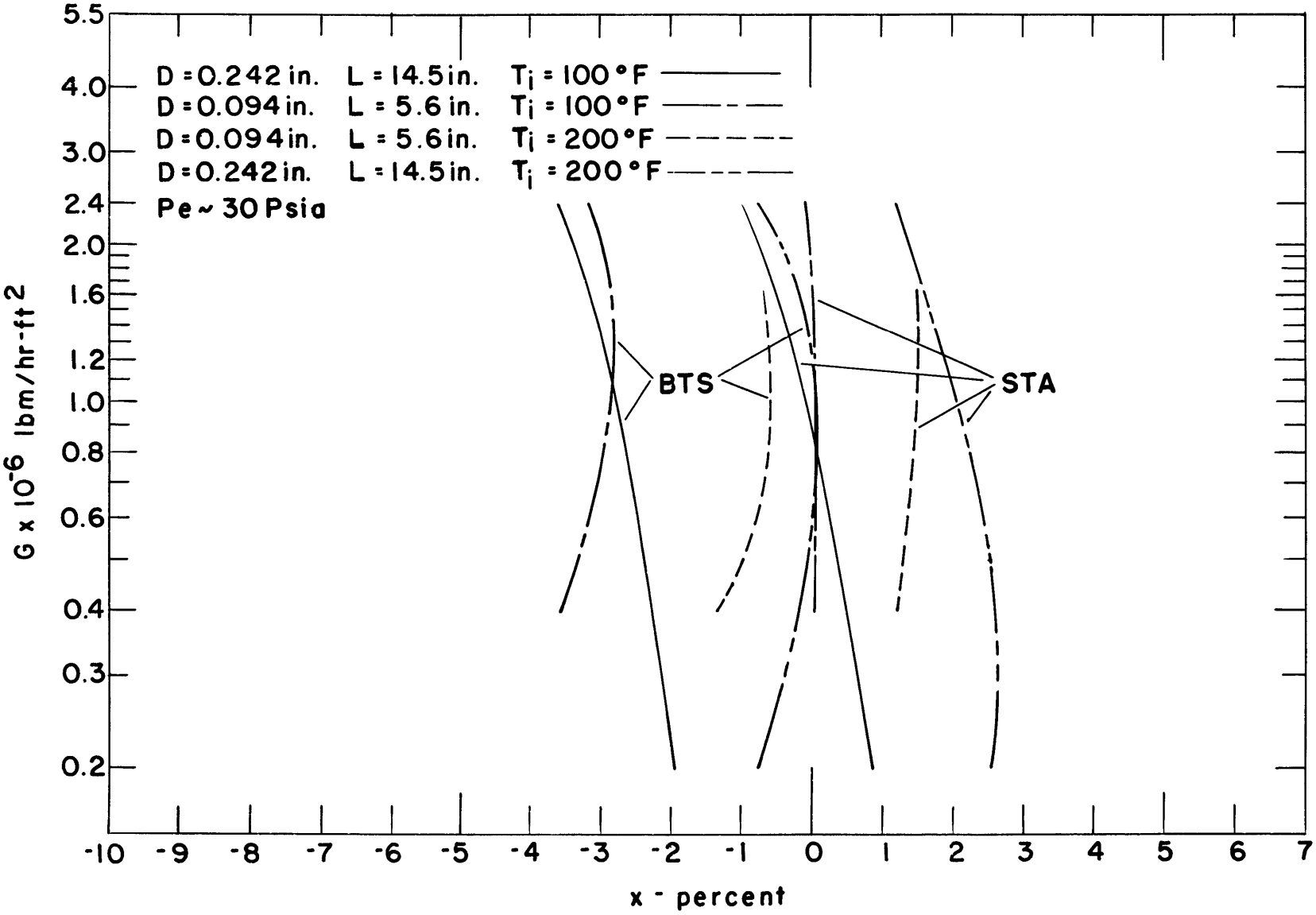

FIG. 26 EFFECT OF DIAMETER ON FLOW REGIME BOUNDARIES

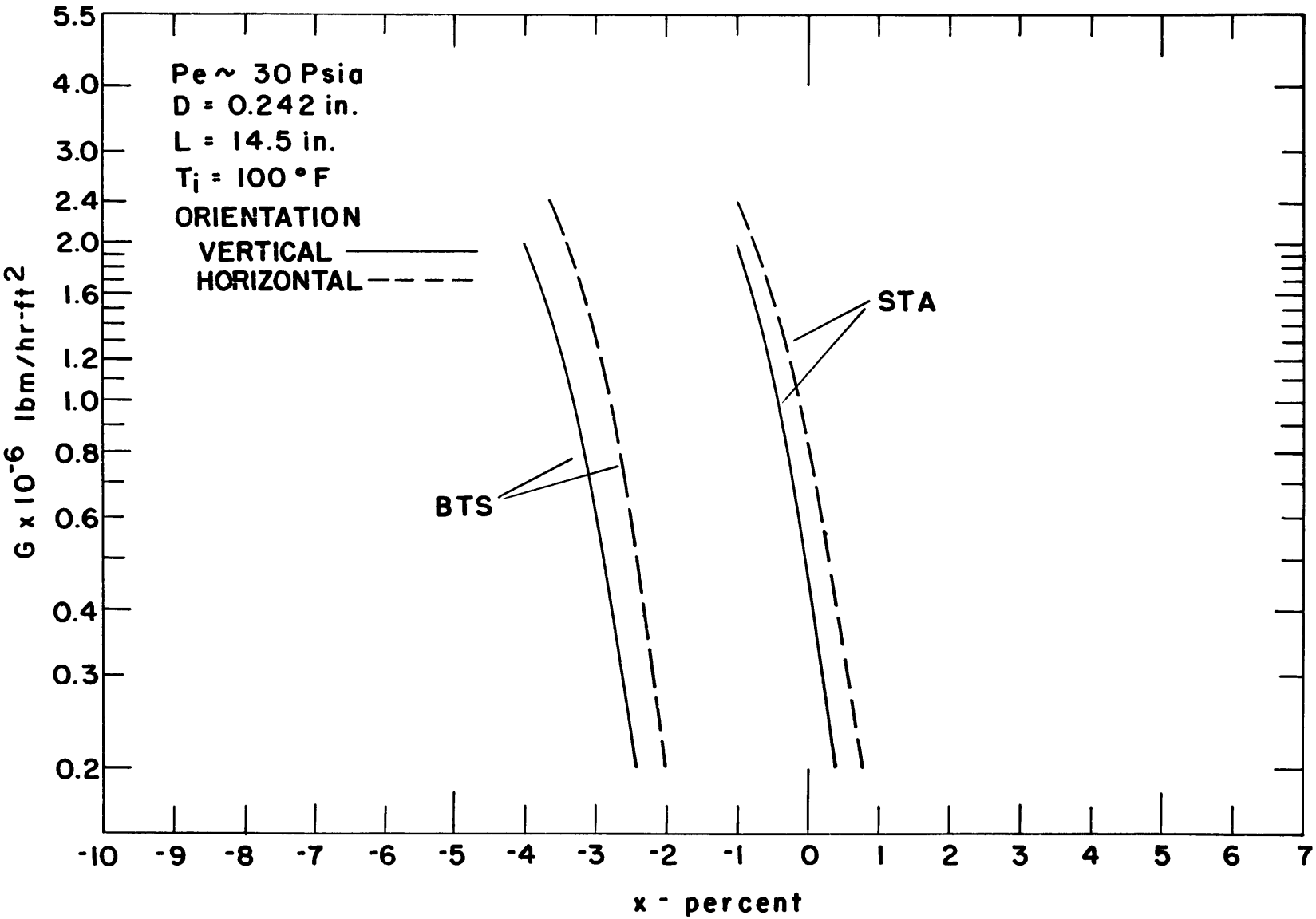

FIG. 27 EFFECT OF ORIENTATION ON FLOW REGIME BOUNDARIES

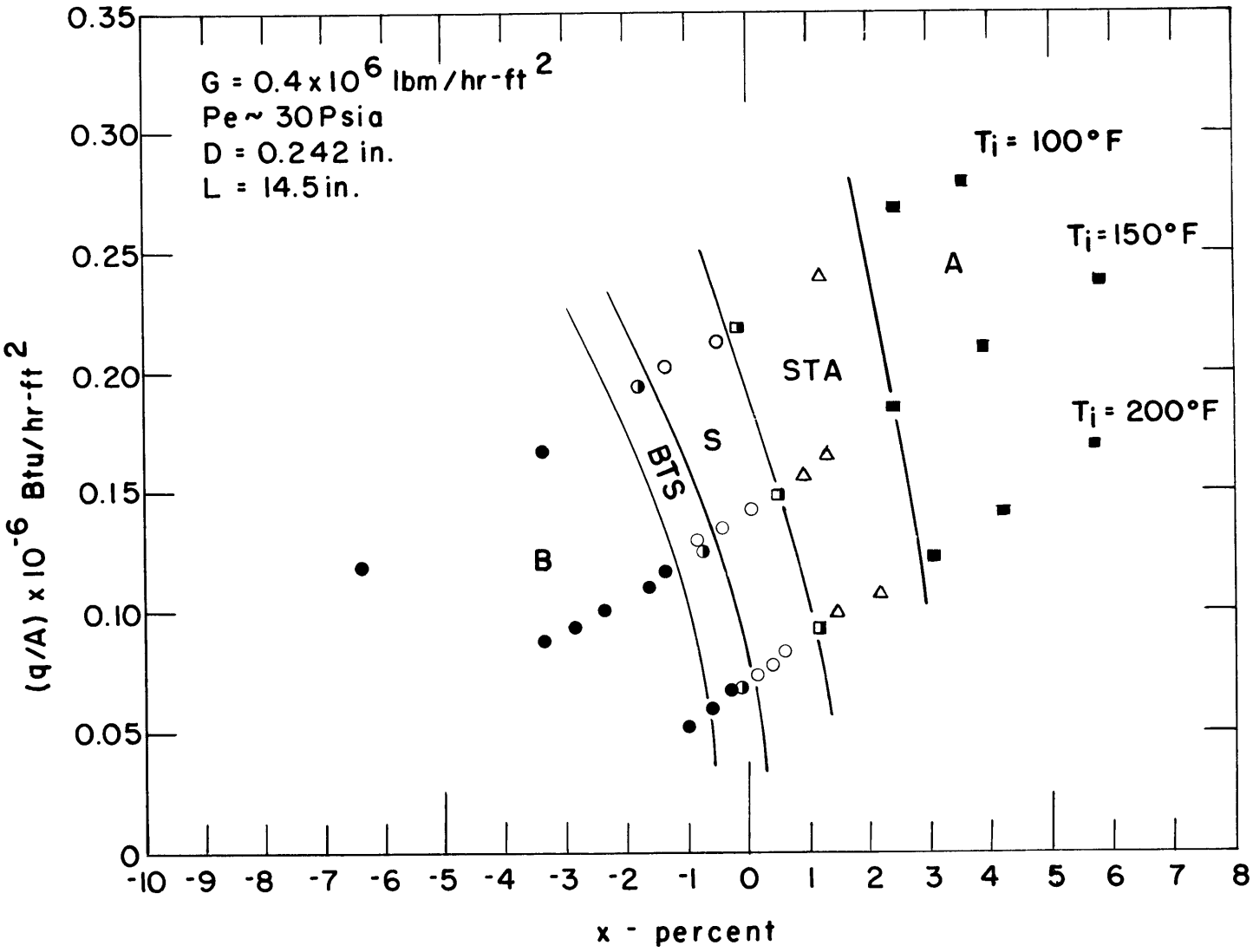

FIG. 28 FLOW REGIME MAP ON HEAT FLUX vs. QUALITY CO-ORDINATES - G = 0.4 X 10^6 lbm/hr-ft^2, LOW PRESSURE

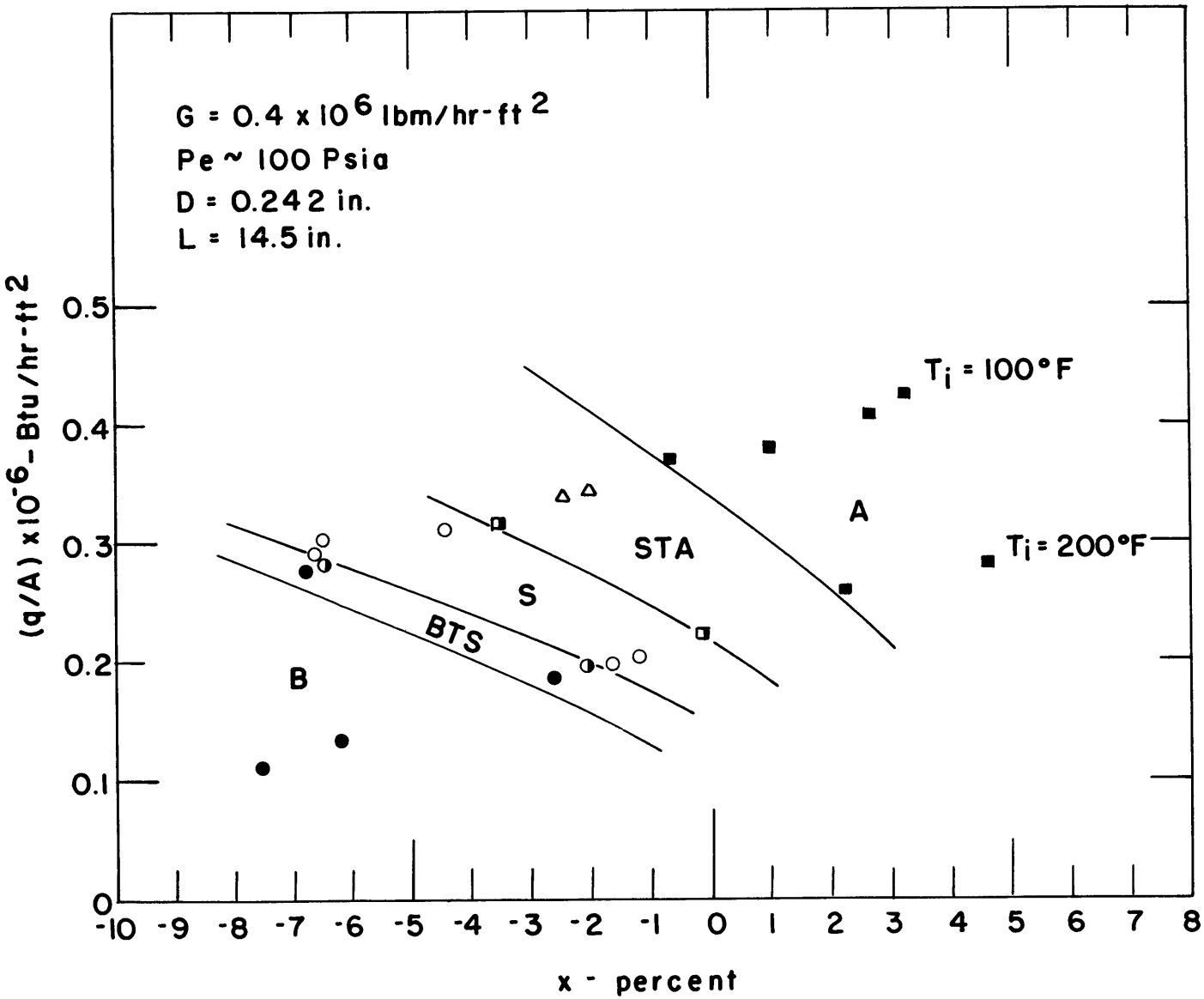

FIG. 29 FLOW REGIME MAP ON HEAT FLUX vs. QUALITY CO-ORDINATES - G = 0.4 X 10^6 lbm/hr-ft^2, HIGH PRESSURE

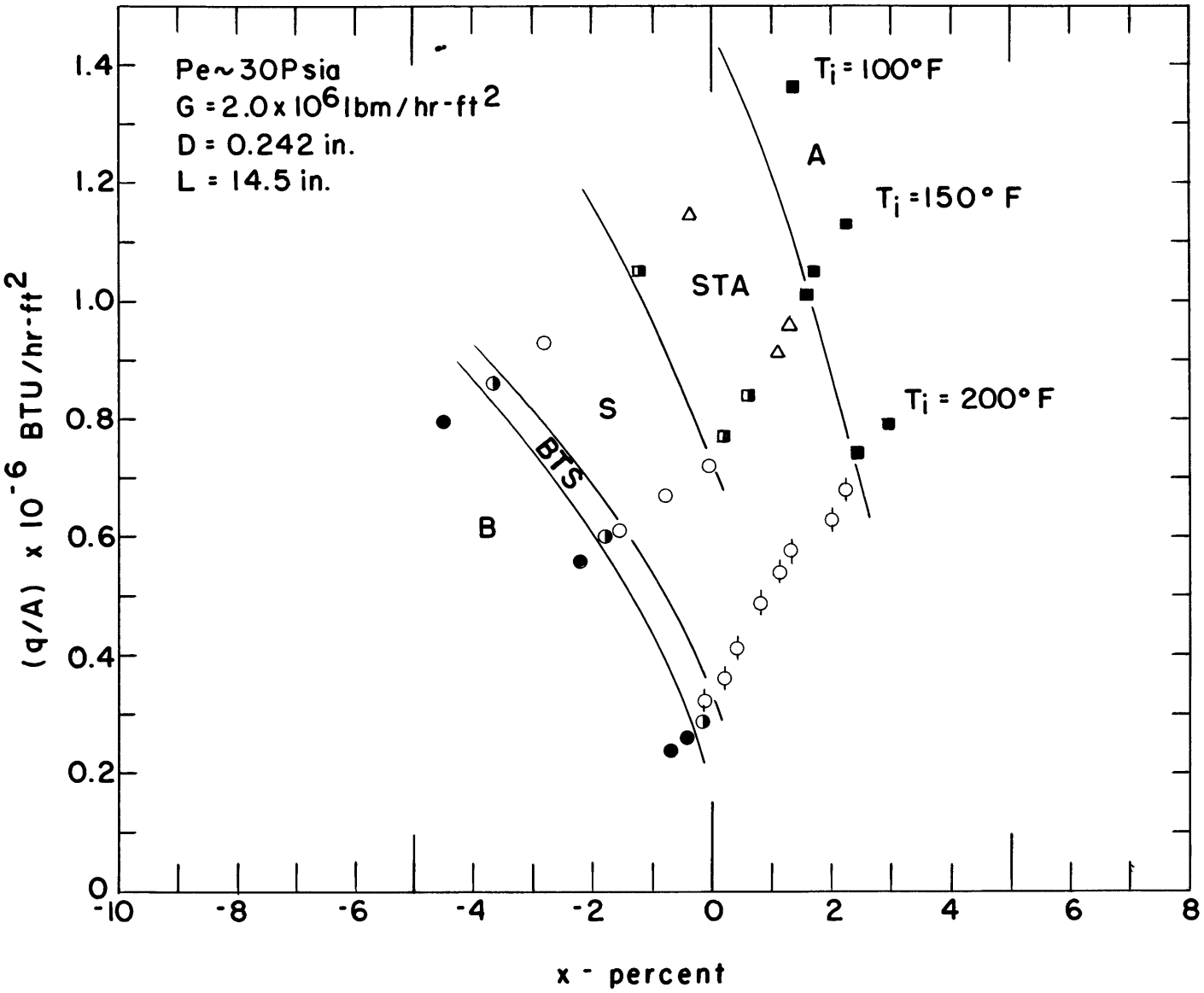

FIG. 30 FLOW REGIME MAP ON HEAT FLUX vs. QUALITY CO-ORDINATES - G = 2.0 X 10^6 lbm/hr-ft^2, LOW PRESSURE

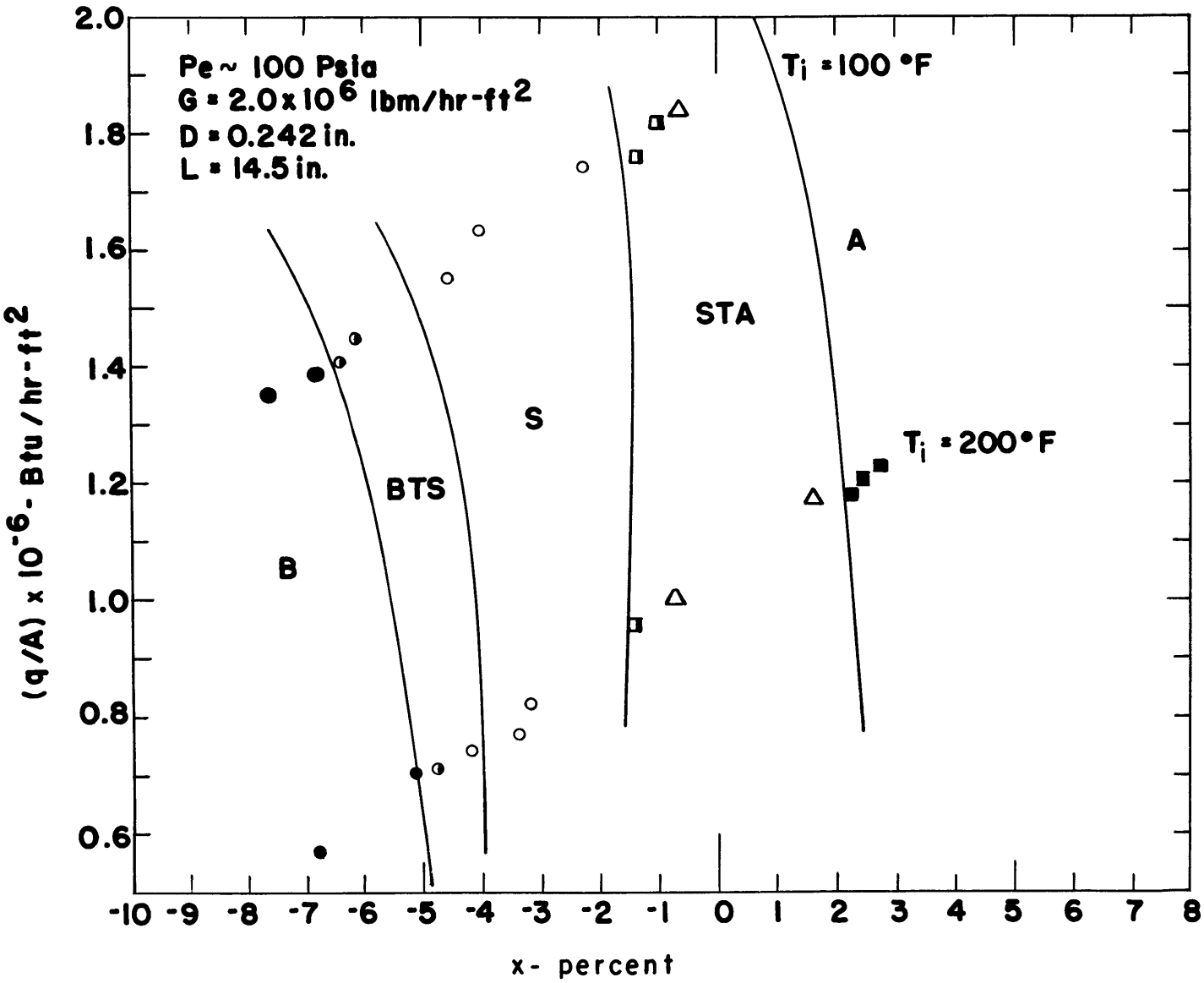

FIG. 31 FLOW REGIME MAP ON HEAT FLUX vs. QUALITY CO-ORDINATES - G = 2.0 X 10^6 lbm/hr-ft^2, HIGH PRESSURE

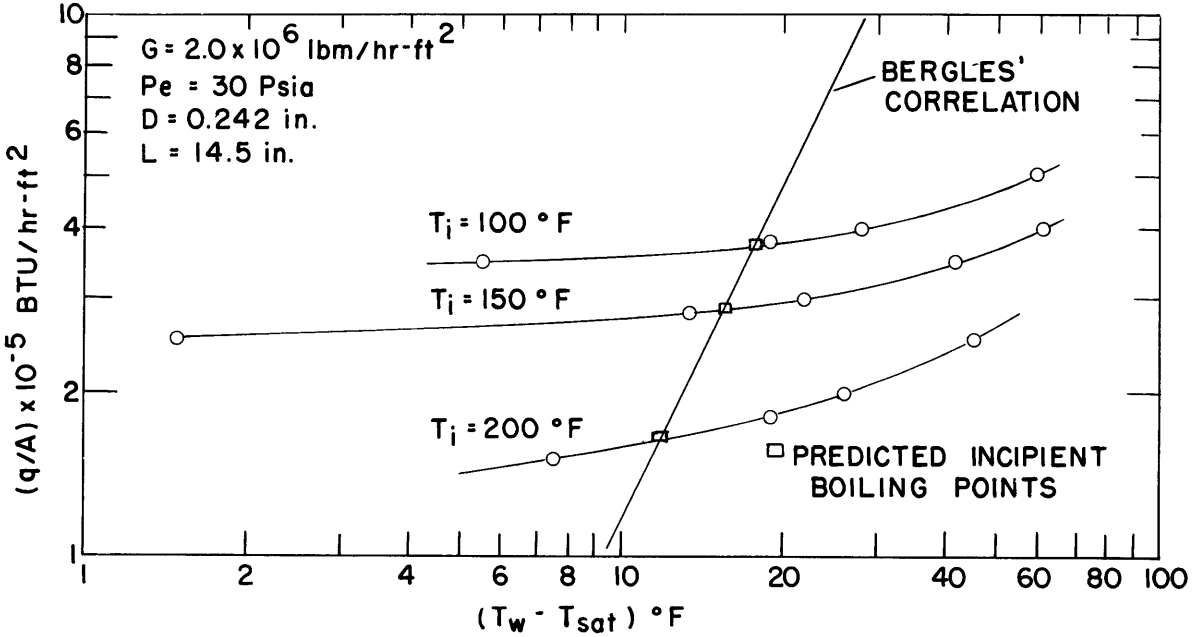

FIG. 32a INCIPIENT BOILING CALCULATIONS

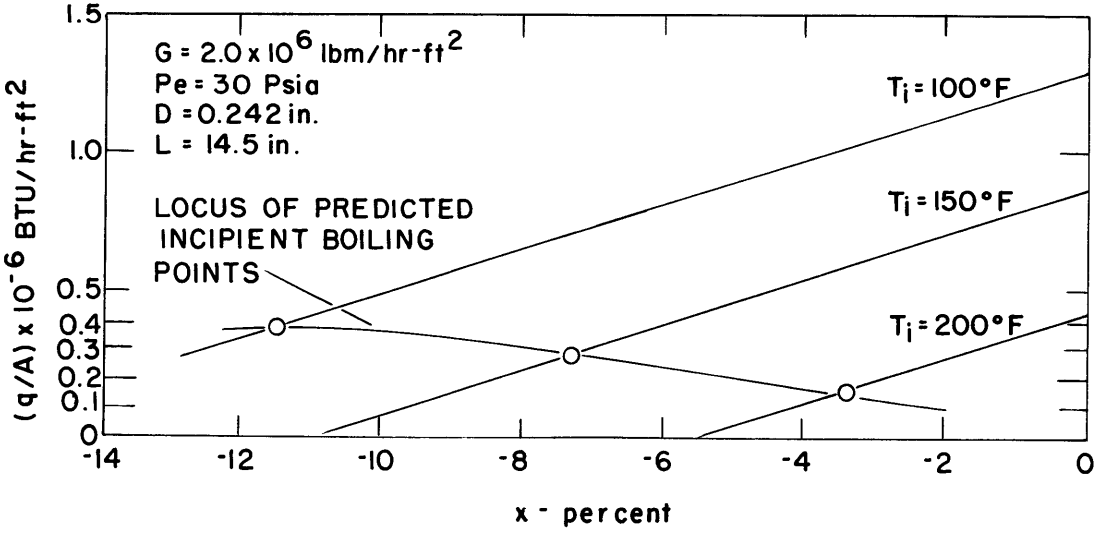

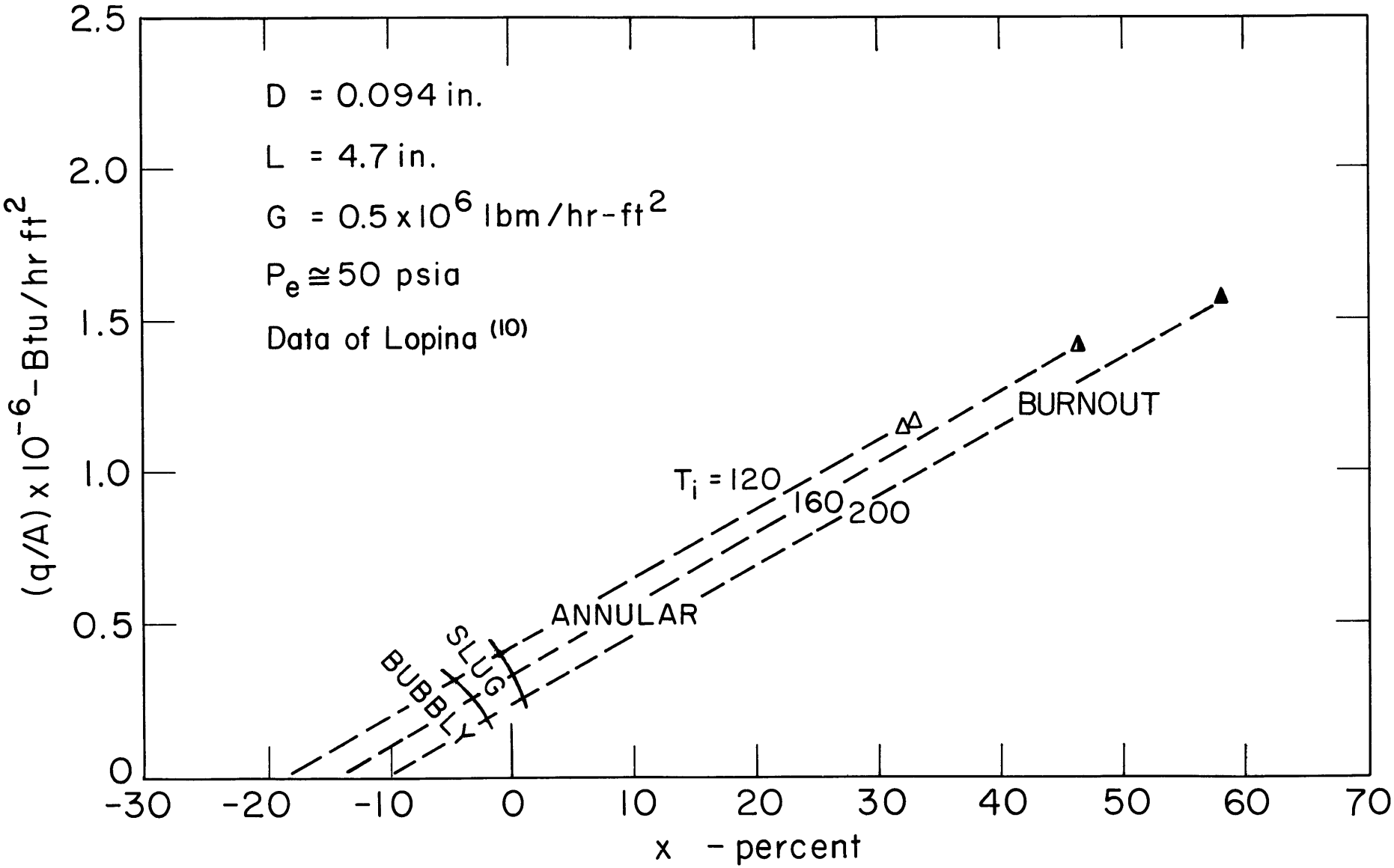

FIG. 33 OPERATING LINES AND FLOW PATTERNS FOR TYPICAL CRITICAL HEAT FLUX DATA

BIBLIOGRAPHY

1. Gouse, S.W. Jr., "An Introduction to Two-Phase Gas Liquid Flow" MIT Engineering Projects Laboratory Report 8734-3, June, 1964.

2. Baker, Ovid, "Simultaneous Flow of Oil and Gas," Oil and Gas Jour., Vol. 53, 1954, pp. 185-195.

3. Martinelli, R.C., and D.B. Nelson, "Prediction of Pressure Drop During Forced-Circulation Boiling of Water", Trans. ASME, Vol. 70, 1948, pp. 695-702.

4. Lavin, J.G., and E.H. Young, "Heat Transfer to Evaporating Refrigerants in Two-Phase Flow", AICHE reprint of paper presented at the Symp. on Two-Phase Flow and Heat Transfer, Memphis, Tenn., Feb. 2-5, 1964.

5. Griffith, P., "Two-Phase Flow-Regime Detection", ASME Paper No. 64-WA/HT-43.

6. Hsu, Y.Y., and R.W. Graham, "A Visual Study of Two-Phase Flow in a Vertical Tube with Heat Addition", NASA TN D-1564, January, 1963.

7. Suo, M., A.E. Bergles, E.F. Boyle, L. Clawson and P. Goldberg, "Investigation of Boiling Flow Regimes and Critical Heat Flux" Dynatech Corporation Report, NYO-3304-3, March 1, 1965.

8. Bergles, A.E., and M. Suo, "Investigation of Boiling Water Flow Regimes at High Pressures", Dynatech Corporation Report, NYO-3304-8, 1966.

9. Bennett, A.W., G.F. Hewitt, J.G. Collier, R.K.F. Keeys, P.M.C. Lacey, "Flow Visualization Study of Boiling at High Pressure", AERE-R4874, 1965.

10. Lopina, R.F., "Two-Phase Critical Heat Flux to Low Pressure Water Flowing in Small Diameter Tubes", SM Thesis, Dept. of Mech. Eng., MIT, June, 1965.

11. Vohr, J.H., "Flow Patterns of Two-Phase Flow - A Survey of Literature", TID 11514, AEC, December, 1960.

12. Kepple, R.R., and T.V. Tung, "Two Phase (Gas-Liquid) System Heat Transfer and Hydraulics (An Annotated Bibliography)", ANL-6734, July, 1963.

13. Solomon, J.V., "Construction of a Two-Phase Flow Regime Transition Detector", SM Thesis, Dept. of Mech. Eng., MIT, June, 1962.

14. Nassos, G.P., "Development of an Electrical Resistivity Probe for Void Fraction Measurements in Air Water Flow", ANL-6738, June, 1963.

15. Haberstroh, R.D., and P. Griffith, "The Transition from the Annular to the Slug Flow Regime in Two-Phase Flow", MIT Engineering Projects Laboratory Report 5003-28, July, 1964.

16. Griffith, P., "The Slug-Annular Flow Regime at Elevated Pressure", ANL-6796, November, 1963.

17. Bergles, A.E., and W.M. Rohsenow, "Forced Convection Surface Boiling Heat Transfer and Burnout in Tubes of Small Diameter", MIT Engineering Projects Laboratory Report 8767-21, May, 1962.

18. Keily, D.P., Meteorology Dept., MIT, Personal Communication, August 12, 1965.

19. Vonnegut, B., A. Doyle, and D. Moffet, "Behavior of Evaporating Electrically Charged Droplets", Jour. of Colloid Science, Vol. 19, 1964, p. 136.

20. Suo, M., Mechanical Engineering Department, MIT, Personal Communication, May, 1965. Professor Suo's calculations were based on Glasstone's, "Physical Chemistry".

21. Radovcich, N.A., and R. Moissis, "The Transition From Two-Phase Bubble Flow to Slug Flow", MIT Engineering Project Laboratory Report 7-7673-22, June, 1962.

22. Bergles, A.E., and W.M. Rohsenow, "The Determination of Forced-Convection Surface Boiling Heat Transfer", Trans. ASME, Jour. of Heat Transfer, Vol. 86, 1964, pp. 365-372.

23. Bowring, R.W., "Physical Model, Based on Bubble Detachment, and Calculation of Steam Voidage in the Subcooled Region of a Heated Channel", Report HPR 10, OECD Halden Reactor Project, December, 1962.

24. Hewitt, G.F., H.A. Hearsey, P.M.C. Lacey, and D.J. Pulling, "Burnout and Film Flow in the Evaporation of Water in Tubes", AERE-R 4864, March, 1965.

25. Todreas, N.E., and W.M. Rohsenow, "The Effect of Non-Uniform Axial Heat Flux Distribution", MIT Engineering Projects Laboratory Report No. 9843-37, September, 1965.

26. Rohsenow, W.M., and H. Choi, Heat, Mass, and Momentum Transfer, Prentice-Hall, 1963.

27. ElWakil, M.M., Nuclear Power Engineering, McGraw-Hill, 1962.